TESS survey of rotational and pulsational variability of mercury-manganese stars

O. Kochukhov, V. Khalack, O. Kobzar, C. Neiner, E. Paunzen, J. Labadie-Bartz, A. David-Uraz

Monthly Notices of the ROYAL ASTRONOMICAL SOCIETY

MNRAS **506,** 5328–5344 (2021) https://doi.org/10.1093/mnras/stab2107
Advance Access publication 2021 July 22

TESS survey of rotational and pulsational variability of mercury–manganese stars

O. Kochukhov [1★], V. Khalack,[2] O. Kobzar,[2] C. Neiner [3], E. Paunzen [4], J. Labadie-Bartz [5] and A. David-Uraz [6,7]

[1]*Department of Physics and Astronomy, Uppsala University, Box 516, SE-75120 Uppsala, Sweden*
[2]*Département de Physique et d'Astronomie, Université de Moncton, Moncton, NB E1A 3E9, Canada*
[3]*LESIA, Paris Observatory, PSL University, CNRS, Sorbonne Université, Université de Paris, 5 place Jules Janssen, F-92195 Meudon, France*
[4]*Department of Theoretical Physics and Astrophysics, Masaryk University, Kotlářská 2, CZ-611 37 Brno, Czech Republic*
[5]*Instituto de Astronomia, Geofísica e Ciencias Atmosféricas, Universidade de Sào Paulo, Rua do Matão 1226, Cidade Universitãria, Sáo Paulo, SP 05508-900, Brazil*
[6]*Department of Physics and Astronomy, Howard University, Washington, DC 20059, USA*
[7]*Center for Research and Exploration in Space Science and Technology, and X-ray Astrophysics Laboratory, NASA/GSFC, Greenbelt, MD 20771, USA*

Accepted 2021 July 19. Received 2021 July 19; in original form 2021 June 13

ABSTRACT

Mercury–manganese (HgMn) stars are late-B upper main sequence chemically peculiar stars distinguished by large overabundances of heavy elements, slow rotation, and frequent membership in close binary systems. These stars lack strong magnetic fields typical of magnetic Bp stars but occasionally exhibit non-uniform surface distributions of chemical elements. The physical origin and the extent of this spot formation phenomenon remain unknown. Here, we use 2-min cadence light curves of 64 HgMn stars observed by the *Transiting Exoplanet Survey Satellite* (*TESS*) during the first 2 yr of its operation to investigate the incidence of rotational modulation and pulsations among HgMn stars. We found rotational variability with amplitudes of 0.1–3 mmag in 84 per cent of the targets, indicating ubiquitous presence of star-spots on HgMn-star surfaces. Rotational period measurements reveal six fast-rotating stars with periods below 1.2 d, including one ultra-fast rotator (HD 14228) with a 0.34-d period. We also identify several HgMn stars showing multiperiodic g-mode pulsations, tidally induced variation and eclipses in binary systems.

Key words: binaries: close – stars: chemically peculiar – stars: early-type – stars: oscillations – stars: rotation – starspots.

1 INTRODUCTION

Mercury–manganese (HgMn) stars correspond to one of the subclasses of the heterogeneous group of chemically peculiar (CP) stars, found on the upper main sequence. These objects are generally characterized by a significant deviation of their surface chemical composition from the solar abundance pattern. HgMn stars have spectral types from B6 to A0, corresponding to the effective temperature range from 16 000 to 10 000 K, and are distinguished by strong lines of ionized Hg and/or Mn, discernible in low-resolution classification spectra (e.g. Paunzen, Hümmerich & Bernhard 2021b). These line strength anomalies indicate an overabundance of these chemical elements by up to 6 orders of magnitude relative to their solar abundances. High-resolution spectroscopic analyses of HgMn stars also reveal large overabundances of Xe, Ga, Pt, Au, and many other heavy elements (e.g. Castelli & Hubrig 2004; Yüce & Adelman 2014; Ghazaryan, Alecian & Hakobyan 2018) whereas He and CNO elements are often observed to be underabundant (Roby & Lambert 1990). HgMn stars are frequently found in spectroscopic binaries (Gerbaldi, Floquet & Hauck 1985) and rotate slower than normal stars of the same temperature (Abt, Levato & Grosso 2002).

HgMn stars are traditionally assigned to the non-magnetic (CP3) sub-group of chemically peculiar stars according to the classification proposed by Preston (1974). CP3 stars are qualitatively different from the magnetic Bp stars (CP2 sub-group), which occupy the same region in the Hertzsprung–Russell diagram. Magnetic Bp stars also exhibit highly unusual surface element abundances, but possess kG-strength, globally organized, stable magnetic fields. The presence of these fields leads to a stationary non-uniform distribution of chemical elements with height in stellar atmosphere and laterally across the stellar surface (e.g. Michaud, Charland & Megessier 1981; Babel & Michaud 1991; LeBlanc et al. 2009; Alecian 2015). This, in turn, results in a high-amplitude spectroscopic (e.g. Kochukhov et al. 2004, 2014; Kochukhov, Shultz & Neiner 2019) and photometric (Jagelka et al. 2019) rotational modulation. In contrast to this spectacular and well-studied variability of CP2 objects, HgMn stars were considered to be some of the least variable early-type stars (Adelman 1998). Most attempts to detect magnetic fields on their surfaces yielded negative results (e.g. Shorlin et al. 2002; Wade et al. 2006; Aurière et al. 2010; Kochukhov et al. 2011; Makaganiuk et al. 2011b; Bagnulo et al. 2012, 2015; Martin et al. 2018). Occasional reports of magnetic detections in HgMn stars (e.g. Hubrig et al. 2010, 2012, 2020)

★ E-mail: oleg.kochukhov@physics.uu.se

remain inconclusive since in every such case re-analyses of the same data (Makaganiuk et al. 2011a, 2012; Kochukhov et al. 2013) or independent observations (Folsom et al. 2010) failed to confirm the presence of the field. The most sensitive magnetic field studies of HgMn stars have reached a longitudinal field precision of a few G for bright narrow-line HgMn stars, proving that they do not host global fields comparable in strength to those found in magnetic Bp stars. This, however, does not exclude the presence of ultra-weak sub-G fields of the type found in Vega, Sirius and several hot Am stars (Petit et al. 2010, 2011; Blazère et al. 2016).

Despite the absence of magnetic field, the notion of constancy of HgMn stars has been challenged by high-precision spectroscopic observations. It turned out that some HgMn stars show a low-amplitude rotational modulation of spectral line profiles. This variability is consistent with the presence of low-contrast spots of, typically, those chemical elements which show the largest overabundances (e.g. Adelman et al. 2002; Kochukhov et al. 2005; Hubrig et al. 2006; Briquet et al. 2010; Kochukhov et al. 2011; Makaganiuk et al. 2011b, 2012; Korhonen et al. 2013; Strassmeier et al. 2017). Remarkably, it was also discovered that the geometry of chemical spots on HgMn stars evolves with time (Kochukhov et al. 2007; Korhonen et al. 2013). In comparison, higher contrast surface inhomogeneities on magnetic Bp stars show no temporal changes on time-scales of at least several decades. These observations offer an intriguing possibility that the structure formation in HgMn stellar atmospheres is governed by a hitherto unknown variety of dynamic atomic diffusion process (Alecian, Stift & Dorfi 2011), which is distinct from the magnetically controlled atomic diffusion operating in magnetic Bp stars (Michaud, Alecian & Richer 2015).

The incidence of spots on HgMn stars remains largely undetermined. Rotational line profile variability was detected in a relatively small number of the brightest HgMn stars that could be observed with high signal-to-noise ratio ground-based spectroscopy. Rotational periods were securely measured from these data for only four objects. High-precision photometric observations from space opened another avenue for finding variable HgMn stars. Detection of variability with periods of a few days was reported for individual HgMn stars using CoRoT (Morel et al. 2014; Strassmeier et al. 2017), Kepler (Balona et al. 2011, 2015), K2 (White et al. 2017; Krtička et al. 2020), the BRITE nanosat constellation (Strassmeier et al. 2020), and *Transiting Exoplanet Survey Satellite* (*TESS*; Balona et al. 2019; González et al. 2021). In some of these cases, interpretation of photometric variability in terms of rotational modulation was supported by the detection of line profile variations in follow-up time-resolved spectroscopy. In other cases variability could not be unambiguously ascribed to spots (Hümmerich et al. 2018) and interpretation in terms of g-mode pulsations was preferred (Alecian et al. 2009). Recent studies identified another cause of variability of some HgMn stars – the ellipsoidal and heartbeat variation associated with the orbital motion in a close binary system (Kochukhov et al. 2021; Paunzen et al. 2021a). To summarize, variability of HgMn appears to be ubiquitous and diverse, emphasizing the necessity of advancing from case studies of individual objects to statistical analyses of meaningful stellar samples.

The full-sky survey carried out by the *TESS* (Ricker et al. 2015) enables the first systematic unbiased investigation of the photometric variability of HgMn stars. The goal of our study is to take advantage of this unique research opportunity by performing a comprehensive assessment of the information content of the *TESS* light curves of HgMn stars observed during the first 2 yr of mission operation. Using these data, we identify periodic signals, associate them with rotational modulation or stellar pulsations, and assess the incidence of these variability phenomena among HgMn stars. The paper is organized as follows: Section 2 introduces observational data and target selection, Section 3 provides details of our time series analysis, Section 4 presents results of this analysis for stars with rotational modulation (Section 4.1), pulsations (Section 4.2), and photometric variation related to binarity (Section 4.3). The paper is concluded by Section 5, which summarizes and discusses our work.

2 OBSERVATIONAL DATA AND TARGET SELECTION

This study is based upon the observations collected by the *TESS* satellite during the first 2 yr of its operation. In this period, lasting from 2018 July 25 to 2020 July 4, *TESS* has surveyed most of the sky in 26 pointings, commonly referred to as sectors. Sectors 1–13 covered the Southern ecliptic hemisphere whereas the remaining sectors (14–26) correspond to observations of targets North of the ecliptic equator. Observations within each sector were carried out continuously for 27.4 d, except for a small gap in the middle of each sector. Depending on the ecliptic latitude, targets were observed for a minimum of 27.4 d (one sector) and up to about 1 yr (13 sectors). Here, we used the 2-min cadence PDCSAP (pre-search data conditioning simple aperture photometry) light curves provided by the *TESS* science team and available for download from the Mikulski Archive for Space Telescopes (MAST).[1] Details of data processing steps included in the pipeline that produced these light curves can be found in Jenkins et al. (2016). The pixel scale of *TESS* is 21 arcsec per pixel and typical apertures used by the pipeline are 3–7 pixels across, resulting in signal integration over 1–2 arcmin. With such large effective apertures contamination by nearby sources may be of concern.

To find HgMn stars with 2-min *TESS* light curves, we first constructed a unified catalogue of all known stars with this chemical peculiarity type. We started by extracting all objects with Hg and/or Mn spectral peculiarity from the general *Catalogue of Ap, HgMn, and Am stars* (Renson & Manfroid 2009). The resulting list was complemented with HgMn stars identified by Chojnowski et al. (2020) based on *SDSS*/APOGEE spectra and by Paunzen et al. (2021b) using LAMOST DR4 data. A compilation of HgMn abundance analyses (Ghazaryan & Alecian 2016; Ghazaryan, Alecian & Hakobyan 2018) as well as a number of recent studies reporting discovery of individual HgMn stars (e.g. Catanzaro et al. 2010, 2020; Monier, Gebran & Royer 2015; Monier et al. 2019; Sikora, Wade & Rowe 2020; González et al. 2021) were also taken into account. These selection steps resulted in a catalogue containing 544 definite and probable HgMn stars brighter than $V = 12$ mag. This list of targets was cross-matched with the revised *TESS* Input Catalogue (TIC; Stassun et al. 2019) in order to find TIC identification numbers and stellar magnitudes. The TIC numbers were then used to query MAST. For 71 stars from our list 2-min light curves were obtained during the first 2 yr of the *TESS* mission. After further examination of the information and literature on these stars, TIC 99025917 (HD 193772) and TIC 174194250 (HD 220885) were removed since these are well-known magnetic Ap stars with 'Hg' or 'Mn' listed in their spectral peculiarity field in Renson & Manfroid (2009). Likewise, TIC 118573876 (HD 22128) has 'Mn' in its peculiarity type in this catalogue, but is known to be an SB2 system containing two cool Am stars (Folsom, Wade & Johnson 2013). Furthermore, TIC 29715050 (HD 179709B), TIC 868508027 (HD 82984B), and TIC 358467049

[1] https://mast.stsci.edu

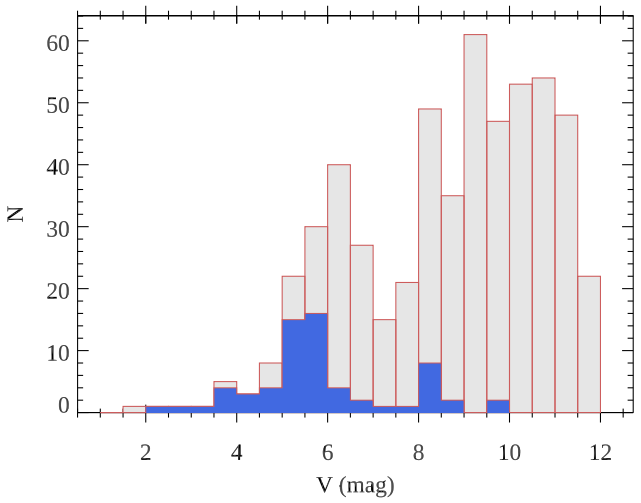

Figure 1. Distribution of V magnitudes of HgMn stars analysed in this study (dark histogram bars) relative to all known stars of this type (light histogram bars).

(CPD-60 944B) are fainter secondary components in close visual binaries unresolved by *TESS*. These objects were not considered since their light curves are likely dominated by variability of the non-HgMn primaries.

The final sample of targets analysed in this study comprises 65 objects listed in Table A1. Their V magnitudes range between 2.1 and 9.7, with a median value of 5.6. The magnitude distribution of the studied stars relative to the initial HgMn-star sample is shown in Fig. 1. The studied sample is reasonably representative of HgMn stars brighter than $V \approx 6$ but is highly incomplete for fainter stars.

Considering a coarse pixel scale of *TESS*, we assessed contamination of all 65 targets by examining *Gaia* eDR3 (Gaia Collaboration 2021) sources contributing to the apertures used to derive the light curves for each studied star. Three targets – TIC 121161014 (HD 133833), TIC 163024899 (HD 99803), TIC 307291308 (HD 71066) – were found to have contaminating sources 2.1–3.5 mag fainter than the main target. Contamination is negligible for the remaining stars.

3 TIME SERIES ANALYSIS

Our assessment of the information content of *TESS* light curves of HgMn stars was carried out using standard time series analysis techniques: examination of the generalized Lomb Scargle (GLS) periodograms (Zechmeister & Kürster 2009) and least-squares model fitting in the time domain. Prior to these analysis steps, cadences marked as low quality in the *TESS* data files were excluded. Then, GLS periodograms were computed for frequencies up to the Nyquist limit and examined visually. The frequency positions and heights of peaks corresponding to obvious periodic signals were read off the GLS periodogram and adopted as initial guesses for subsequent non-linear least-squares model fitting in the time domain. In this fitting, implemented with the help of the MPFIT package written in IDL (Markwardt 2009), the frequencies, amplitudes, and phases of all harmonic signals included in the model were adjusted simultaneously. Whenever periodogram showed evidence of higher order harmonics (as is very common for a non-sinusoidal rotational modulation), the frequencies of these signals were fixed to multiples of the first harmonic and only amplitudes and phases were adjusted. Applying this constrained fitting to all harmonic components simultaneously provided a more precise determination of the fundamental frequency.

After initial satisfactory fit in the time domain was achieved, we subtracted the resulting model from the data and calculated GLS periodogram of the residuals in order to reveal further low-amplitude periodic signals. The significance of periodogram peaks was assessed using the canonical S/N ≥ 4 criterium (Breger et al. 1993; Kuschnig et al. 1997), with the noise floor determined as described by Shultz et al. (2021). Any additional harmonic signals found in this way were added to the model and optimization of the model parameters by fitting the light curve in the time domain was repeated with new frequencies taken into account. This process was continued until no further significant frequencies were evident in the periodogram of the residuals. Formal parameter errors derived by the least-squares fitting algorithm were adopted as uncertainty estimates for the amplitudes and frequencies of periodic signals included in the model.

TESS light curves exhibit several types of instrumental artefacts, including slow drifts and occasional significant deviations at the beginning and/or end of 13.7 d continuous data segments. Strongly deviating light-curve sections were manually removed prior to the GLS periodogram calculation and least-squares fitting. To account for the drifts, we approximated the background stellar brightness with low-order (typically 1–3) polynomials, fitting their coefficients simultaneously with harmonic signals. The background of each 13.7 d segment was treated independently from other segments. The high-order polynomials were typically applied in the presence of a clear short-period variation, otherwise the straight-line background was used to avoid removing variation with a period comparable to the segment's length. This piecewise polynomial background was removed before producing the final light curve and periodogram plots presented below.

A few of our targets discussed in more detail in Section 4.3 exhibit abrupt changes of brightness due to transits or eclipses. Harmonic analysis is poorly suited for this type of variability. Since the main focus of our study is investigation of the rotational and pulsational variability of HgMn stars, we removed parts of light curves affected by transits and eclipses prior to the time series analysis described above. When multiple eclipses were observed, their times were found by computing the centroid time of each event and the period of an eclipsing binary was estimated by a linear fit to the times of individual events (separately for the primary and secondary eclipses).

4 RESULTS

4.1 Rotational variability

Photometric rotational variability of HgMn stars is expected to occur due to low-contrast chemical abundance spots present on the surfaces of these stars (e.g. Prvák, Krtička & Korhonen 2020). Given the typical 27.4-d length of most *TESS* data sets and the methodology of the time series analysis adopted in our study, in particular the independent treatment of slow drifts within individual 13.7 d light-curve segments, we are not sensitive to rotational modulation exceeding periods of ≈ 13 d. On the other end, frequencies higher than about 2 d^{-1} are unlikely to be related to stellar rotation. Consequently, candidate rotational signals were searched in the 0.5–13 d period range. Rotational photometric modulation of CP stars is frequently non-sinusoidal (e.g. Jagelka et al. 2019). Therefore, the presence of a low-frequency periodogram peak accompanied by harmonic frequencies was considered to be a tell-tale sign of rotational variability.

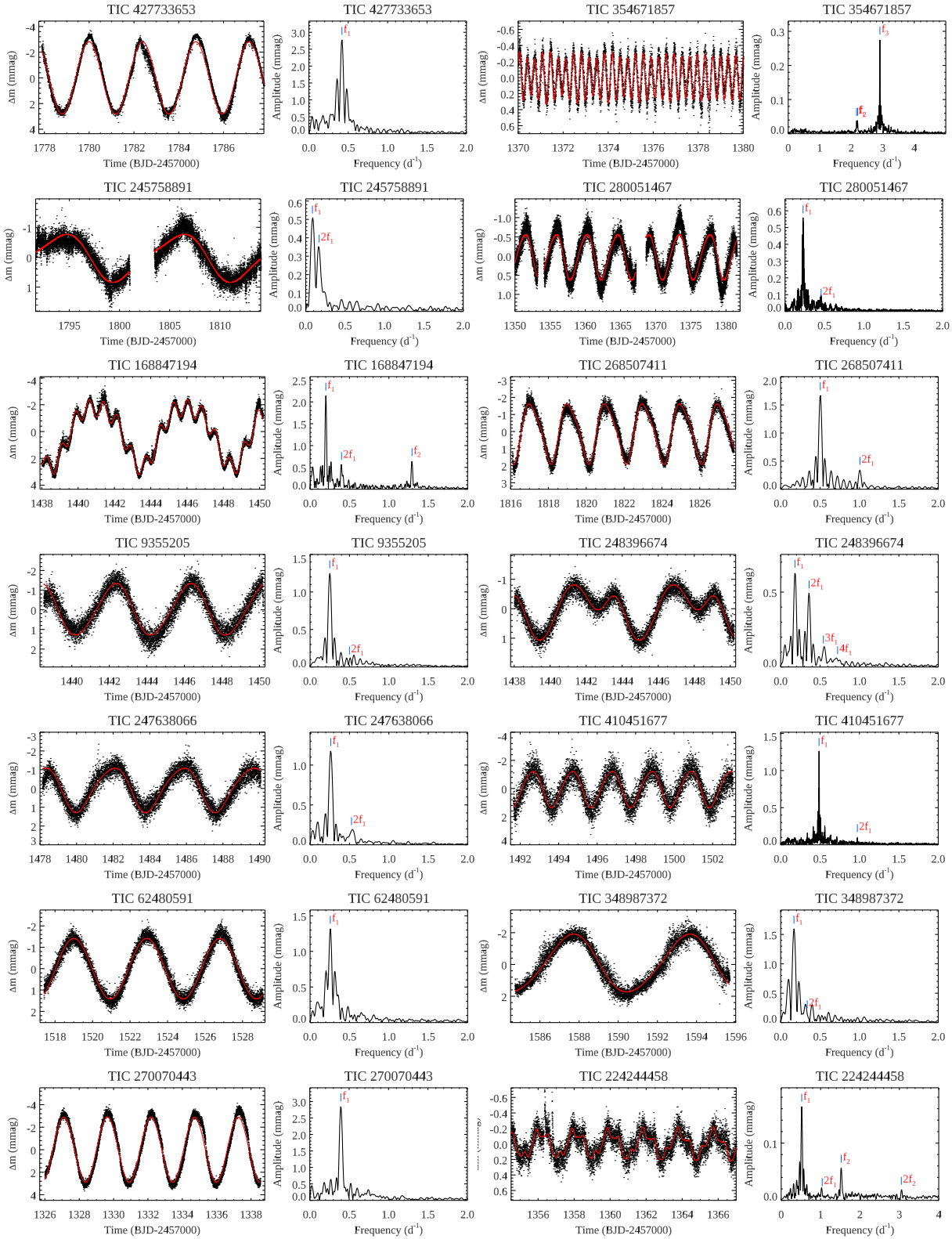

Figure 2. Examples of HgMn stars showing clear rotational variability. For each target, the left-hand panels show a section of the *TESS* light curve (points) together with the harmonic model fit (solid line). The right-hand panels show the associated periodogram with significant frequencies identified by short vertical bars.

In this study, we were able to detect photometric variability compatible with rotational modulation for 55 target stars. For 44 of them a single low-frequency peak, often accompanied by harmonics, dominated the GLS periodogram. Representative examples of such photometric behaviour, corresponding to a range of light-curve complexity and variability periods, are presented in Fig. 2. We assign these targets to the group exhibiting definite rotational modulation (identified by 'ROT' in Table A1). For 11 other stars with low am-

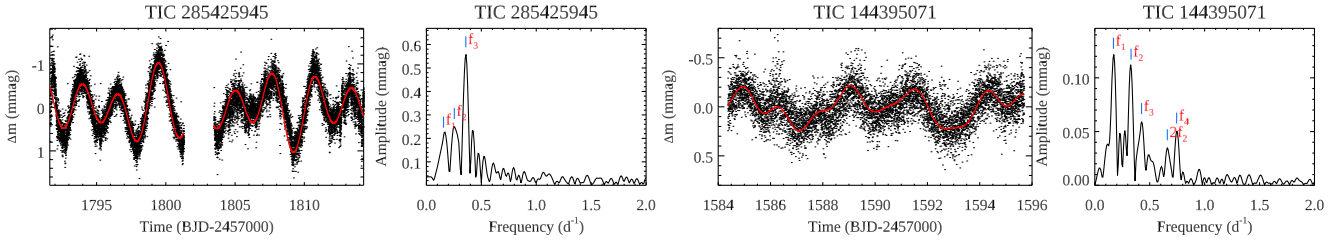

Figure 3. Same as Fig. 2, but for the cases when rotational modulation cannot be unambiguously identified among multiple low-frequency signals present in the data.

plitudes of photometric variability in the *TESS* band and/or multiple low-frequency periodogram peaks of comparable amplitude (Fig. 3), our identification of rotational variability is tentative. These objects are marked by 'ROT?' in Table A1. That table summarizes results of our detailed frequency analysis, including derived amplitudes and periods, for all significant signals present in *TESS* light curves of studied stars. For five stars lacking coherent periodic signals an upper amplitude limit in the 0–2 d^{-1} frequency range is provided. Below we comment on some of the most interesting rotationally variable stars included in our study.

TIC 427733653 (HD 358, α And, Fig. 2) was one of the first HgMn stars for which conclusive evidence of spectroscopic rotational variability was found and a surface map of chemical abundance spots was reconstructed (Ryabchikova et al. 1999; Ilyin 2000; Adelman et al. 2002; Kochukhov et al. 2007). The spectroscopic rotational period of 2.38195(3) d is close to, but is formally inconsistent with, the 2.3834(2) d period derived here from *TESS* observations. As demonstrated by Kochukhov et al. (2007), the surface spot distribution in α And evolves slowly with time. This may introduce additional uncertainties in the spectroscopic period determination, which have not been fully accounted for. With a semi-amplitude of 2.8 mmag, α And exhibits the strongest photometric rotational variability among the bona fide HgMn stars included in this study.

TIC 285425945 (HD 11291, 2 Per, Fig. 3). This star is known to be an SB1 system with an orbital period of 5.627 d (Pourbaix et al. 2004). The *TESS* light curve shows multiple low frequency signals. The highest amplitude one, corresponding to 2.784 d, is tentatively attributed to rotational modulation. Given that this signal is close to half of the orbital period, interpretation in terms of ellipsoidal variability (Kochukhov et al. 2021) cannot be excluded either.

TIC 229099027 (HD 11753, φ Phe) is a well-known spectroscopically variable HgMn star with evolving surface distributions of chemical elements (Briquet et al. 2010; Makaganiuk et al. 2012; Korhonen et al. 2013). It is a member of a long-period, potentially eclipsing, SB1 system with $P_{\rm orb} = 1126$ d (Pourbaix et al. 2013). The rotational period found in spectroscopy, $P_{\rm rot} = 9.531$ d, is longer than the 9.324(1) d period that provides the best description of the *TESS* light curve of this star. This discrepancy can be understood in the context of weak solar-like differential rotation reported by Korhonen et al. (2013). The photometric rotational variability observed in the *TESS* band is complex with the second harmonic dominating the periodogram and up to four harmonics necessary to provide a satisfactory description of the light curve. The same *TESS* data set of HD 11753 was assessed by Prvák et al. (2020). These authors demonstrated that the observed photometric amplitude is well matched by their theoretical calculations using abundance maps available for this HgMn star, although the detailed shape of the light curve could not be reproduced.

TIC 354671857 (HD 14228, φ Eri, Fig. 2). Variability of this star was detected in previous studies based on *TESS* data (Balona et al. 2019; Pedersen et al. 2019). The periodogram shows a prominent peak at $P = 0.344$ d and weaker signals at 0.45–0.46 d. This star is an extremely rapid rotator with $v_{\rm e}\sin i = 240$ km s^{-1} (Hutchings, Nemec & Cassidy 1979) and the 0.344 d variability is fully compatible with rotational modulation. This star is by far the fastest rotator in our study. It is consistently referred to as an HgMn star in the literature (Schneider 1981; Renson & Manfroid 2009), but its classification needs to be confirmed by a modern spectroscopic study since finding a chemical peculiarity at such extreme rotation rate is unexpected.

TIC 280051467 (HD 19400, θ Hyi, Fig. 2). This is a rare PGa-type CP star, which is considered to be the hotter extension of HgMn stars (Alonso et al. 2003). A subtle spectroscopic variability was reported for this object by Hubrig et al. (2014), though no rotational period was derived. The *TESS* data analysed in our study shows a clear variability with $P_{\rm rot} = 4.369$ d. Detection of this rotational modulation was also mentioned by Balona et al. (2019) and Pedersen et al. (2019).

TIC 168847194 (HD 27376, 41 Eri, Fig. 2) is an SB2 system with nearly equal-mass components and an orbital period of 5.010 d (Hummel et al. 2017). Both components show chemical peculiarities characteristic of HgMn stars (e.g. Dolk, Wahlgren & Hubrig 2003) and both exhibit spectroscopic variability (Hubrig et al. 2012). Rotation of the components is expected to be synchronized with the orbital rate, which is confirmed by our measurement of $P_{\rm rot} = 5.010$ d using *TESS* data. Interestingly, the *TESS* light curve of 41 Eri also shows a sinusoidal signal at 0.77 d suggesting that one of the components may exhibit pulsational variability.

TIC 373026963 (HD 28217, HR 1402). The spectroscopic variability of this star was reported by Nuñez, González & Hubrig (2010) and Hubrig et al. (2011), but the rotational period remained unknown. According to our analysis, $P_{\rm rot} = 3.132$ d.

TIC 268507411 (HD 28929, HR 1445, Fig. 2). This HgMn star shows a clear photometric variation with $P_{\rm rot} = 1.989$ d. Previous ground-based and space photometric observations yielded a somewhat shorter 1.977-d period (Paunzen et al. 2013; Netopil et al. 2017).

TIC 9355205 (HD 30963) was recently identified as an HgMn star by Monier et al. (2019). This star shows rotational variability with a period very close to 4 d. An independent analysis of *TESS* data by David-Uraz et al. (2021) retrieved the same period and did not find magnetic field based on follow up spectropolarimetric observations.

TIC 436723855 (HD 31373, HR 1576) shows rotational modulation with $P_{\rm rot} = 1.448$ d as well as a weaker low-frequency sinusoidal signal at 2.644 d. No photometric variability was detected for this star by Adelman & Brunhouse (1998) and Paunzen et al. (2013) whereas

Pope et al. (2019) classified this object as an SPB star based on *K2* observations.

TIC 248396674 (HD 32964, 66 Eri, Fig. 2) is another SB2 HgMn star with a mass ratio close to one. In contrast to 41 Eri, only one of the components exhibits HgMn spectral peculiarities and line profile variability (Yushchenko et al. 1999; Makaganiuk et al. 2011b). The *TESS* light curve of this star shows a complex double-wave shape with up to four harmonic evident in the periodogram. The most recent determination of the orbital period yields $P_{\rm orb} = 5.523$ d (Hubrig et al. 2012). This is close, but not identical, to $P_{\rm rot} = 5.535$ d derived from *TESS* photometry.

TIC 169534653 (HD 33904, μ Lep) is one of the brightest HgMn stars showing rotational line profile variability (Nuñez et al. 2010; Kochukhov et al. 2011). Here, we report the first conclusive determination of the rotational period for this star, $P_{\rm rot} = 2.933$ d. The period of 2 d mentioned by Netopil et al. (2017) is not supported by *TESS* data.

TIC 116333643 (HD 37519). No photometric variability was detected in this star by Paunzen et al. (2013) using *STEREO* satellite observations. On the other hand, the *TESS* light curve shows a clear non-sinusoidal variation with $P_{\rm rot} = 0.841$ d. This is the second shortest rotational period found in our study. It cannot be excluded that this signal is coming from an unresolved companion star. However, HD 37519 is not known to be a binary and its very rapid rotation is consistent with the high projected rotational velocity, $v_{\rm e}\sin i = 195$ km s^{-1}, reported by Abt et al. (2002).

TIC 247638066 (HD 38478, 129 Tau, Fig. 2) rotates with a period of 3.806 d. Paunzen et al. (2013) listed this object as constant.

TIC 155095401 (HD 49606, 33 Gem). Different periods, ranging between 1.4 and 3.3 d, were reported for this star (Glagolevskij, Panov & Chunakova 1985; Paunzen et al. 2013; Netopil et al. 2017). None of them corresponds to the period determined here using *TESS* observations, $P_{\rm rot} = 8.546$ d. This star was recently found to be part of an SB1 system with an orbital period of 148.3 d (Catanzaro et al. 2016).

TIC 148109427 (HD 53244, γ CMa) is a bright HgMn star with spectral variability investigated by several studies (Briquet et al. 2010; Nuñez et al. 2010; Hubrig et al. 2011). Briquet et al. (2010) determined $P_{\rm rot} = 6.16$ d, which is somewhat shorter than the 6.214-d period measured here. Burssens et al. (2020) concluded that γ CMa shows rotational modulation with a period of 6.250 d based on the same *TESS* data set.

TIC 410451677 (HD 66409, Fig. 2) exhibits clear rotational variability with $P_{\rm rot} = 2.055$ d. The presence of this rotational modulation was also noted by Balona et al. (2019) and Pedersen et al. (2019) based on a smaller subset of *TESS* observations. Weak spectroscopic variability of this HgMn star was discussed by Nuñez et al. (2010).

TIC 307291308 (HD 71066, κ^2 Vol) was not conclusively detected as variable by Pedersen et al. (2019). However, Balona et al. (2019) and this study attribute the 1.296-d periodicity seen in the *TESS* light curve of this star to rotational modulation. This star is known to have sharp spectral lines (e.g. Kochukhov et al. 2013), which would be compatible with the short period only if the target is seen nearly pole-on. Alternatively, the observed signal could be explained by contamination by a 2.1-mag fainter nearby star HD 71046C, which is blended with HD 71066 in *TESS* images.

TIC 62480591 (HD 75333, 14 Hya, Fig. 2) shows variability with $P_{\rm rot} = 3.894$ d according to our analysis. Netopil et al. (2017) reported a rotational period of 6 d, which is incompatible with our measurement.

TIC 319809753 (HD 101189, HR 4487) exhibits spectral variability that was described in several studies (Hubrig et al. 2011, 2012, 2020) but the rotational period remained undetermined. The *TESS* data allowed us to establish $P_{\rm rot} = 2.004$ d. This is very close to an integer number of days, making interpretation of ground-based observations challenging.

TIC 348987372 (HD 106625, γ Crv, Fig. 2) is the second brightest HgMn star after α And. Its *TESS* light curve exhibits a clear variation with $P_{\rm rot} = 5.938$ d. No previous reports of its variability, using either photometric or spectroscopic observations, can be found in the literature.

TIC 144395071 (HD 110073, HR 4817, Fig. 3) shows multiple low-frequency peaks. The second highest one, corresponding to $P_{\rm rot} = 3.030$ d, is tentatively attributed to rotational modulation since this signal is non-sinusoidal. Alternatively, the 5.903-d signal could also correspond to rotation. Spectroscopic variability of this star was reported by Nuñez et al. (2010) and Hubrig et al. (2011).

TIC 442652828 (HD 141556, χ Lup) is known to be an SB2 system with $P_{\rm orb} = 15.25$ d (Le Bouquin et al. 2013) and with a tertiary component also present. A relatively short rotational period of 1.793 d derived from *TESS* data is unexpected for the sharp-line HgMn primary and may originate from one of the other two components.

TIC 51612589 (HD 145842, θ Nor). For this newly identified HgMn star González et al. (2021) reported the 1.087-d period based on the same observational data as analysed here. Our measurement yields a close period value of 1.086 d.

TIC 323999777 (HD 168733, HR 6870) has discrepant peculiarity classifications in the literature. Most papers describe it as a magnetic CP star (Kochukhov & Bagnulo 2006; Briquet et al. 2007; Collado & López-García 2009), which is supported by the definite detection of a global magnetic field (Mathys 1994; Mathys & Hubrig 1997). A few studies group HD 168733 with HgMn stars based on its chemical abundance pattern (Cowley et al. 2010; Ghazaryan et al. 2018). Variability in the *TESS* light curve of HD 168733 has an unusually high amplitude for an HgMn star and a period of 6.326 d, which is compatible with $P_{\rm rot} = 6.3$ d given by Netopil et al. (2017). This is a clear outlier in our study, suggesting that this object is indeed a magnetic Bp star.

TIC 27901267 (HD 172044, HR 6997) shows a non-sinusoidal rotational modulation with $P_{\rm rot} = 4.330$ d. This star is known to be an SB1 with a 1675-d period (Pourbaix et al. 2004).

TIC 347160134 (HD 174933, 112 Her) is an SB2 system with $P_{\rm orb} = 6.362$ d (Ryabchikova, Zakharova & Adelman 1996). The period derived from *TESS* data, $P_{\rm rot} = 12.419$ d, is approximately twice this value suggesting that the primary rotates sub-synchronously.

TIC 270070443 (HD 198174, HR 7961, Fig. 2) is another object with a high photometric variability amplitude in the *TESS* band (Balona et al. 2019; Pedersen et al. 2019) and historically a somewhat dubious relation to HgMn stars. Our measurement of $P_{\rm rot} = 2.5365(2)$ d is shorter than 2.545 d reported by Paunzen et al. (2013) and Netopil et al. (2017). The former study grouped HR 7961 with HgMn stars. However, its spectral peculiarity class is indicated as undetermined by Renson & Manfroid (2009) and the association with HgMn stars in the literature comes only from UV spectrophotometry (Cucchiaro et al. 1977). Nevertheless, a high-resolution FEROS spectrum available in the ESO archive clearly shows the Hg II 3984 Å line and enhanced Mn II lines, confirming the HgMn classification of this star.

TIC 129533458 (HD 216831, HR 8723) was reported to be a spectroscopically variable HgMn star (Kochukhov et al. 2005). Our analysis establishes that this rotational modulation occurs with a period of 3.471 d, opening prospects for quantitative interpretation of ground-based spectroscopy.

TIC 224244458 (HD 221507, β Scl, Fig. 2) is one of the brightest HgMn stars showing spectroscopic variability due to surface inhomogeneities. Line profile variability in the spectra of this object was investigated by Briquet et al. (2010) and Hubrig et al. (2020). The former study has established a rotational period of 1.93 d, which is in good agreement with $P_{\rm rot} = 1.921$ d found here. Rotational variability using the sector 2 *TESS* light curve was reported by both Balona et al. (2019) and Pedersen et al. (2019). The first of these studies attributed a flare (evident at time 1356.5 in Fig. 2) to the HgMn star. However, our detailed time series analysis reveals the presence of another rotational signal with $P_{\rm rot} = 0.656$ d, indicating that the *TESS* light curve of β Scl is contaminated by the rotational modulation of a companion star. This signal may be coming from the visual companion detected using diffraction-limited imaging (Schöller et al. 2010; Kammerer et al. 2019). A late-type star with such a short rotational period is expected to be very active and is, most likely, responsible for the observed flare.

TIC 359033491 (HD 225289, HR 9110) shows variability with $P_{\rm rot} = 3.254$ d. This period is shorter by about a factor of 2 compared to $P_{\rm rot} = 6.432$ d given by Netopil et al. (2017). Considering that in the *TESS* periodogram the 3.254-d period is accompanied by the second and third harmonics, it is the more likely rotational period.

4.2 Pulsations

Several classes of pulsating variables are known among B-type stars. The two best studied types are the β Cep p-mode pulsators and the slowly pulsating B (SPB) g-mode variables (e.g. Aerts, Christensen-Dalsgaard & Kurtz 2010). The former group of stars typically pulsates with frequencies above ~ 5 d^{-1}; the latter has frequencies below this limit. There are hybrid pulsators exhibiting both p- and g-modes simultaneously (e.g. Buysschaert et al. 2017). The classical short-period β Cep pulsations are found in early-B stars that are significantly hotter than the HgMn stars included in our study. Nevertheless, it is known that late-B stars occasionally also exhibit pulsations with periods typical of β Cep stars. These late-B variable stars are sometimes called 'Maia variables' (Balona et al. 2015; Mowlavi et al. 2016; Balona & Ozuyar 2020), although the supposed prototype of this class, the star Maia (20 Tau, HD 23408), is itself an HgMn star showing rotational modulation due to chemical spots and no pulsations (White et al. 2017). It is beyond the scope of our study to address this confusing nomenclature. In the remainder of this section, we will refer to the low-frequency pulsational signals as 'g modes' and the higher frequency ones as 'p modes' without an attempt to formally classify corresponding pulsational variability. In this study, we also searched for rapid oscillations with frequencies above 50 d^{-1} typical of roAp stars (e.g. Cunha et al. 2019), but no examples of such variability were found.

Seven stars included in our surveys show light curves dominated by multiperiodic pulsational variability. Examples of *TESS* data for these stars and corresponding periodograms are shown in Fig. 4.

TIC 245936817 (HD 29589, 93 Tau, Fig. 4) is a well-established HgMn star (Kochukhov et al. 2005), known to have a faint companion (Hubrig et al. 2001) and showing spectroscopic variability (Hubrig et al. 2011). This star was found to be constant by Paunzen et al. (2013). On the other hand, the *TESS* data reveals a rich spectrum of g modes with periods between 0.27 and 0.75 d. It is plausible that the lowest frequency peak found in our study, corresponding to $P = 1.567$ d, is due to stellar rotation.

TIC 391421890 (HD 93549, HR 4220, Fig. 4) is part of an SB1 system with $P_{\rm orb} = 5.4999$ d (Pourbaix et al. 2004). The *TESS* periodogram shows multiple peaks corresponding to periods in the 1.45–5.65 d range. This variability may be due to a combination of g modes and tidally induced oscillations. The strongest signal at $P_{\rm rot} = 0.874$ d is accompanied by a harmonic and is almost certainly due to rotation. This star has a moderate $v_{\rm e}\sin i$ of 67 km s^{-1} (Zorec & Royer 2012), implying that the inclination angle has to be relatively small for the derived rotational period to be compatible with the radius typical of a late-B star.

TIC 219480018 (HD 145389, φ Her, Fig. 4) is a long-period ($P_{\rm orb} = 565$ d) SB2 system (Zavala et al. 2007) with a narrow-line primary and broad-line secondary. A relatively short rotational period of 3.708 d established by our analysis of the *TESS* light curve is compatible with $v_{\rm e}\sin i = 8$ km s^{-1} measured for the primary if its rotational axis is aligned with the orbital axis. The latter is known to be nearly perpendicular to the plane of the sky ($i_{\rm orb} = 12^\circ$, Zavala et al. 2007). In addition to the rotational modulation signal, there is a cluster of p-mode frequencies around 20 d^{-1}. This p-mode pulsational variability can originate either in the primary or secondary.

TIC 198388195 (HD 156127, Fig. 4) is a recently identified and poorly studied HgMn star that was observed in 12 *TESS* sectors. Owing to this abundance of data, rotational variability with $P_{\rm rot} = 2.459$ d and an amplitude of only 0.11 mmag is firmly established. In addition, this star shows a puzzling group of frequencies at 1.45 d^{-1} as well as second and third harmonics. The main frequency is a quadruplet or, possibly, a quintuplet with the strongest component at $P = 0.6889$ d. The quadruplet components are separated by 0.005365d^{-1}, implying a modulation with a 186-d period. We have no explanation of this unique variability.

TIC 27697099 (HD 171301, HR 6968, Fig. 4) is another HgMn star that, similar to 93 Tau, exhibits multiperiodic g-mode pulsations. The 3.104-d period is likely to be a signature of rotational modulation. At least three significant shorter periods, ranging between 0.63 and 0.95 d, are present in the *TESS* light curve of this star.

TIC 383676357 (HD 172728, HR 7018, Fig. 4) rotates with $P_{\rm rot} = 4.498$ d and shows at least five g-mode pulsation signals with periods in the range of 1.26–2.76 d. This star is not known to be a binary and, thus, represents yet another example of an HgMn star with significant pulsational variability.

TIC 392569763 (HD 173524, 46 Dra, Fig. 4) is an SB2 system with nearly identical components and $P_{\rm orb} = 9.811$ d (Catanzaro & Leto 2004). Both components have chemical anomalies characteristic of HgMn stars (Adelman, Ryabchikova & Davydova 1998; Tsymbal et al. 1998). The *TESS* data for this system shows a clear rotational modulation with a period of 9.827 d. Considering the high precision of the orbital radial velocity and photometric period measurements, the discrepancy with $P_{\rm orb}$ is statistically significant. Nevertheless, this variability is still compatible with rotational modulation produced by one of the (nearly) synchronously rotating HgMn components. In addition, there are three higher frequency signals corresponding to periods in the range of 0.72–1.45 d, indicating that one or both of the components of 46 Dra are g-mode pulsators.

4.3 Binarity

In this section, we summarize time series analysis results for the six targets with variability related to their binary nature. This includes four eclipsing binaries as well as two objects showing heartbeat variation. The light curves and periodograms of these stars are shown in Fig. 5.

TIC 51961599 (HD 5408, HR 266, Fig. 5) is a quadruple system showing the presence of three components in its spectra (Cole et al. 1992). The broad-lined B7IV primary is orbited by a short-period

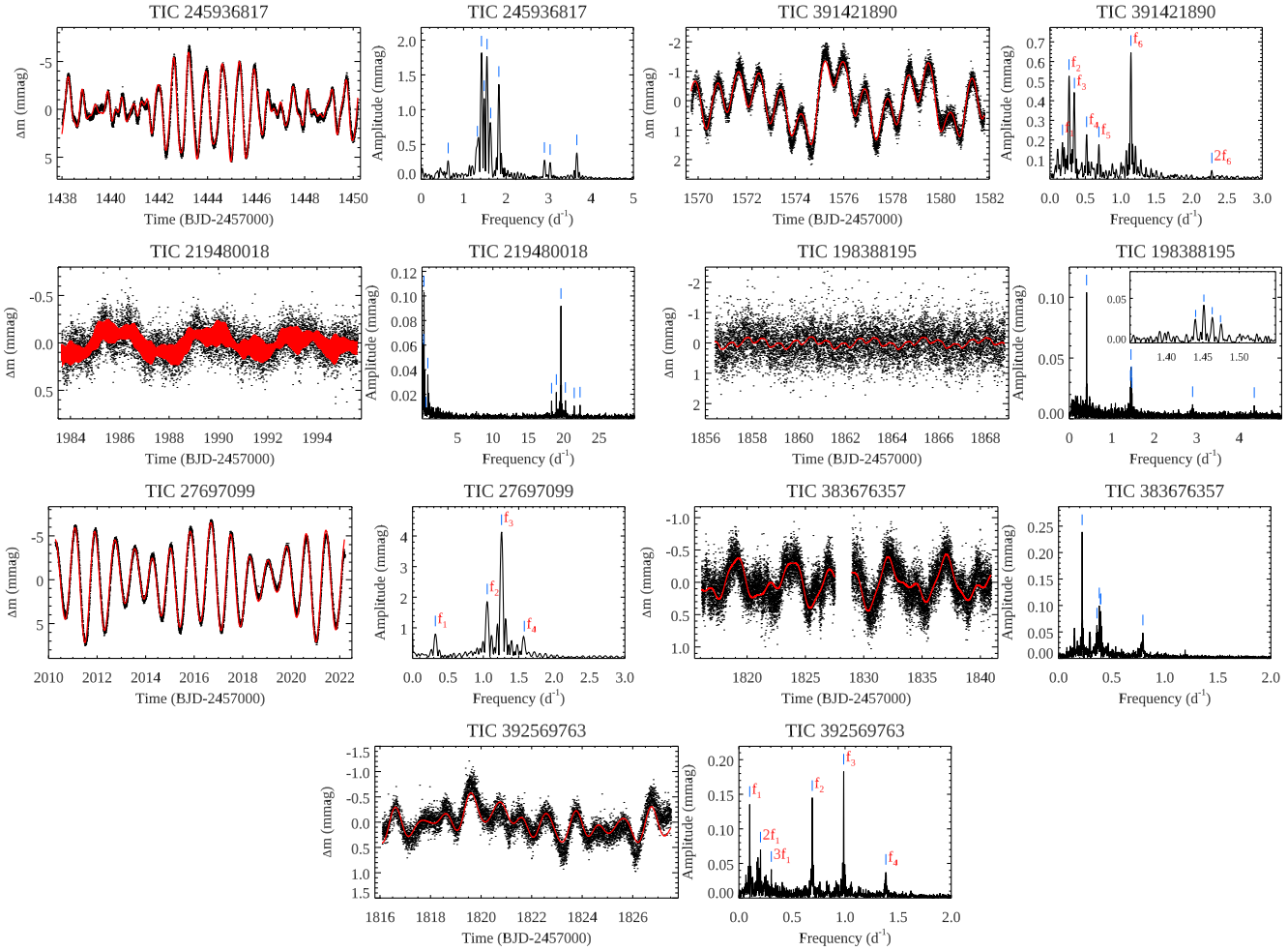

Figure 4. Same as Fig. 2, but for HgMn stars exhibiting significant multiperiodic pulsational variability. For TIC 198388195 the inset shows a non-sinusoidal signal at ≈ 1.45 d^{-1} comprised of a resolved frequency quadruplet.

($P_{\rm orb} = 4.241$ d), eccentric ($e = 0.415$) binary comprising narrow-lined B9IV and A1V components. The B9IV object is classified as an HgMn star. The *TESS* light curve of this system reveals a complex periodic variability with up to 11 harmonics of the 4.241-d period. This signal is thus coming from the tight binary containing the HgMn star, but is inconsistent with a typical eclipse light curve or rotational modulation. Instead, this system appears to show the 'heartbeat' variation caused by dynamic tidal distortions and tidally induced pulsations occurring in close eccentric binary systems, such as those discussed by Thompson et al. (2012). In particular, the *TESS* light curve of HR 266 bears a striking resemblance to the variation of KIC 5034333 discussed in that paper.

TIC 2236015 (HD 34364, AR Aur, Fig. 5) is a well-known double-line eclipsing binary with nearly identical components (e.g. Folsom et al. 2010; Hubrig et al. 2012) and a low-mass unseen tertiary on a wide orbit. The binary has an orbital period of 4.135 d (Albayrak, Ak & Elmasli 2003) with the components rotating synchronously with the orbital motion. The primary shows spectral peculiarities typical of HgMn stars whereas the secondary appears to be a weak Am star (Folsom et al. 2010). Spectral variability in the lines of several heavy elements was detected for the primary (Zverko, Ziznovsky & Khokhlova 1997; Hubrig et al. 2006, 2010; Folsom et al. 2010). The *TESS* light curve of AR Aur shows prominent eclipses, from which we derive an orbital period of 4.134 d consistent with the previous determination. After eclipses are removed, no clear periodic variation can be identified in the residual photometry.

TIC 2776520 (HD 34923, Fig. 5) shows three peaks in its *TESS* periodogram, indicating variation with periods from 0.252 to 0.749 d. This variability is likely to be caused by g-mode pulsations. In addition, a single low-amplitude transit event is observed at BJD = 24571837.8, suggesting that HD 34923 is orbited by a low-mass companion.

TIC 436103335 (HD 36881, HR 1883, Fig. 5) is known to be a long-period ($P_{\rm orb} = 1857$ d), single-line spectroscopic binary (Dworetsky 1982). According to our analysis, the HgMn primary exhibits a rotational variation with $P_{\rm rot} = 1.541$ d. Furthermore, the *TESS* light curve shows evidence of two groups of eclipses, distinguished by different eclipse shapes. From both groups we measured a consistent period of 7.86 d. This leads to the conclusion that the secondary of HR 1883 is an eclipsing binary, consistent with one of the hypotheses considered by Dworetsky (1982) to explain the unusually large mass function derived from the SB1 orbit.

TIC 287287930 (HD 89822, HR 4072, Fig. 5) is an SB2 system with an HgMn primary and an Am secondary (Adelman 1994a). The orbital period is $P_{\rm orb} = 11.579$ d (Pourbaix et al. 2004). The *TESS* light curve of this star displays a coherent variation with $P = 11.581$ d and a complex shape. The periodogram exhibits up to six harmonics,

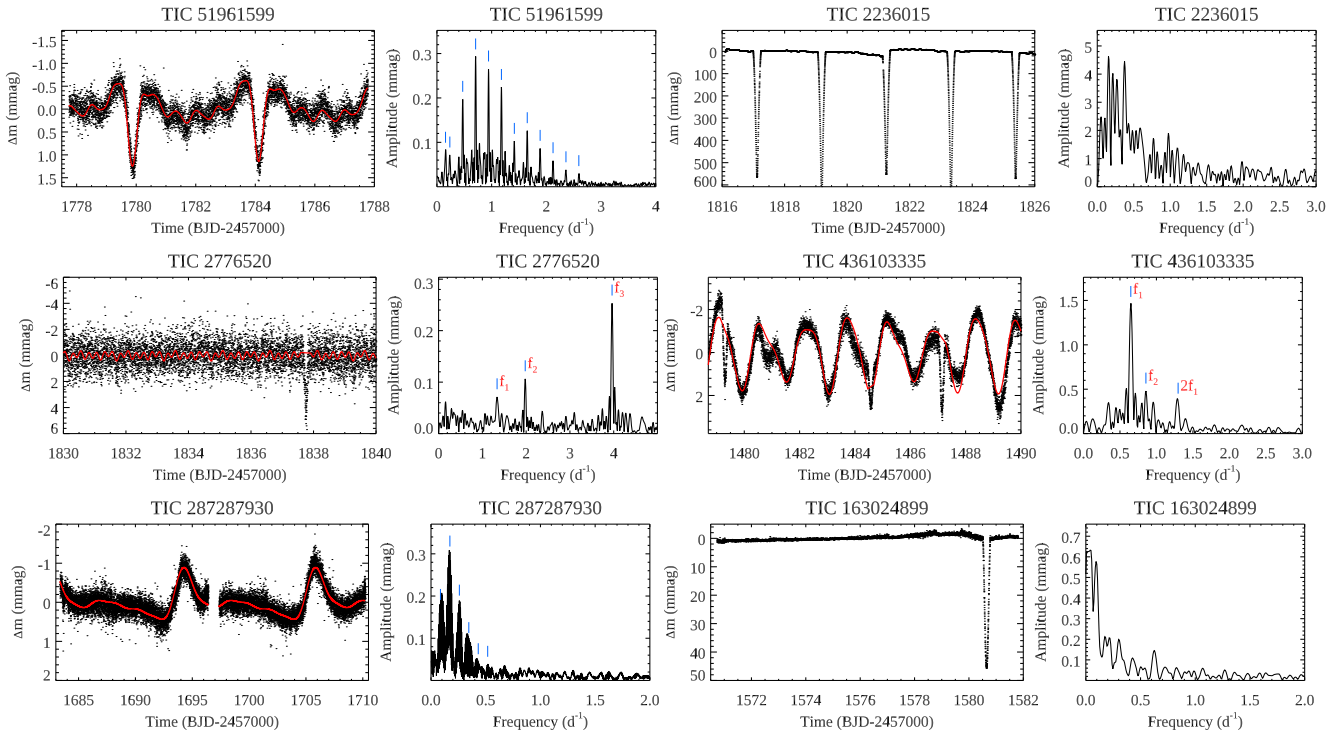

Figure 5. Same as Fig. 2, but for stars with different types of variability related to binarity and/or companions. Periodograms of eclipsing binaries (all targets shown here except TIC 51961599 and TIC 287287930) were computed excluding eclipses.

which is considerably more complex than the signal observed for any rotationally modulated *TESS* light curves of HgMn stars. Taking into account that the orbit of this system is eccentric ($e = 0.26$), it is plausible that the observed behaviour of HR 4072 is another manifestation of the heartbeat variability phenomenon.

TIC 163024899 (HD 99803, HR 4423, Fig. 5) shows a single prominent eclipse in its *TESS* light curve. HR 4423 is known to be a visual binary with a wide enough separation for the components to be resolved by ground-based observations. The secondary is a 2.5 mag fainter Am star (HD 99803B, HIP 56001, Corbally 1984) which is also contributing to the *TESS* light curve. The Bright Star Catalogue (Hoffleit & Warren 1991) entry of HR 4423 mentions a spectroscopic binary nature of the primary. Thus, it is possible that the HgMn component of HR 4423 is a previously unrecognized eclipsing binary.

5 DISCUSSION

We have carried out a systematic search of photometric variability among HgMn stars observed by the *TESS* satellite at 2-min cadence. Light curves of 65 stars classified as HgMn in the literature and observed during cycles 1 and 2 of the mission were examined. Variability consistent with rotational modulation was identified in 55 stars. One of these objects (HD 168733, TIC 323999777) has conflicting peculiarity classifications in the literature and is likely to be a magnetic Bp star. It is distinguished from the rest of the sample by its high variability amplitude. Excluding this target, we derive an 84 per cent (54 out of 64 stars) incidence of rotational modulation in HgMn stars. This shows that such variability is nearly ubiquitous among this class of CP stars and that the majority of them possess low-contrast chemical spots on their surfaces.

Rotational periods measured in our study range from 0.34 to 12.4 d. The median period is 3.77 d. Our period determinations generally agree with the rotational periods deduced in studies of line profile variability using high-resolution time series spectra. This is the case, for instance, for HD 358, HD 11753, HD 32964, HD 53244, and HD 221507. This consistency confirms that both types of variability are linked to the same underlying surface inhomogeneity phenomenon.

Six rapid rotators with periods below 1.2 d were found in our survey (HD 14228, HD 37519, HD 93549, HD 101391, HD 145842, and HD 169027). Such a rapid rotation is not expected for HgMn stars. It was estimated that meridional circulation currents associated with equatorial rotational velocity in excess of ≈90 km s^{-1} would destroy the build up of chemical elements by atomic diffusion (Michaud 1982). This equatorial rotation speed corresponds to a period of 1.4–1.6 d assuming a stellar radius of 2.5–2.9 R$_\odot$ as appropriate for B7–B9 main-sequence stars (Pecaut & Mamajek 2013). Our results challenge the hypothesis of a sharp rotational cutoff of the HgMn phenomenon, but should be verified by confirmation of the HgMn nature of each of these rapid rotators based on high-resolution spectroscopic observations and detailed abundance analysis. This confirmation has already been obtained for HD 169027 by Woolf & Lambert (1999) and for HD 93549 and HD 145842 by González et al. (2021).

The star HD 14228 (TIC 354671857, φ Eri) is particularly puzzling. This is an ultra-fast rotator with $P_{\rm rot} = 0.344$ d, $v_{\rm e}\sin i = 240$ km s^{-1} and a strongly distorted surface (van Belle 2012). Can this really be an HgMn star? Even if it is not confirmed to be a member of this CP-star class, the implications of its prominent rotational variability are still very intriguing. This would mean that at least some normal late-B stars exhibit rotational modulation similar to the behaviour of HgMn stars and hint that non-CP stars also possess a non-uniform surface structure (Balona 2019).

For clarifying if the possible rotational periods found in this study are physical, we have generated the Hertzsprung–Russell diagram of the target star sample. For the $\log T_{\rm eff}$ calibrations, we used the

Johnson *UBV*, Geneva 7-colour, and Strömgren–Crawford *uvbyβ* photometric systems. The individual values were taken from Paunzen (2015) and the General Catalogue of Photometric data.[2] Netopil et al. (2008) introduced calibrations for CP stars using individual corrections for the temperature domain and the CP subclass, which are summarized in their table 2. Here, we follow their approach. For the derivation of the final effective temperatures, all calibrated values were averaged and the standard deviations were calculated. (Table B1).

To calibrate the luminosity, the geometric distances from Bailer-Jones et al. (2021) on the basis of the *Gaia* EDR3 (Riello et al. 2021) were taken. For HD 358 and HD 106625 the distances from the *Hipparcos* mission (van Leeuwen 2007) were applied. For the bolometric correction, the calibration published by Flower (1996) was applied. It is independent of the luminosity and the metallicity. For the bolometric magnitude of the Sun, a value of 4.75 mag (Cayrel de Strobel 1996) was used.

The commonly employed dereddening procedures in the Strömgren–Crawford *uvbyβ* photometric system published by Napiwotzki, Schoenberner & Wenske (1993) was supplemented by the reddening map[3] from Green et al. (2019), which is based on *Gaia* parallaxes and stellar photometry from Pan-STARRS 1 and 2MASS. For the calibrations of the different photometric systems, we used the following relations (Paunzen, Schnell & Maitzen 2006):

$$A_V = 3.1E(B-V) = 4.3E(b-y) = 4.95E(B2-V1). \quad (1)$$

An error value of 0.01 mag was adopted for all objects.

To derive equatorial velocities $v_{\rm eq}$ we used the following equation (Netopil et al. 2017):

$$v_{\rm eq} = 50.579R/P_{\rm rot}, \quad (2)$$

where $v_{\rm eq}$ is in km s^{-1}, R is in solar units, and $P_{\rm rot}$ is in days. This relation requires us to estimate the individual stellar radii. For this we employed the Stellar Isochrone Fitting Tool[4] using the stellar isochrones by Bressan et al. (2012) for $[Z] = 0.014$. To finally get the ratio of the equatorial to the critical equatorial ($v_{\rm crit}$), the latter were taken from Georgy et al. (2013) for the same metallicity as the isochrones.

Netopil et al. (2017) have shown that the majority of the magnetic CP stars show a ratio $v_{\rm eq}/v_{\rm crit}$ of less than 30 per cent with a peak at about 5 per cent. Only a few stars in their sample have values as large as 70 per cent. From our target star sample, 48 out of 55 objects (87 per cent) the ratio falls below 30 per cent. Only one object (HD 36881) has a ratio larger than one, indicating that its period is not due to rotation. Two other stars, HD 14228 and HD 37519, are rotating close to critical velocity ($v_{\rm eq}/v_{\rm crit}$ is 87 and 97 per cent, respectively), which is unusual for CP stars.

In order to get further insights into the statistical characteristics of the rotational variability of HgMn stars, we computed the total effective amplitude by adding in quadrature the amplitudes of all detected harmonics of the rotational frequency (Mikulášek et al. 2007). This effective amplitude is found to be in the range from 0.014 and 2.89 mmag. This parameter is shown as a function of rotational period in Fig. 6. The object with the largest amplitude in this plot, HD 168733, is likely to be a magnetic Bp star. The bona fide HgMn stars with the highest photometric variability are HD 358, HD 28217, and HD 198174. There is no obvious dependence of amplitude on rotational period, but stars with the highest amplitude in the *TESS* band tend to cluster between 2 and 6-d periods.

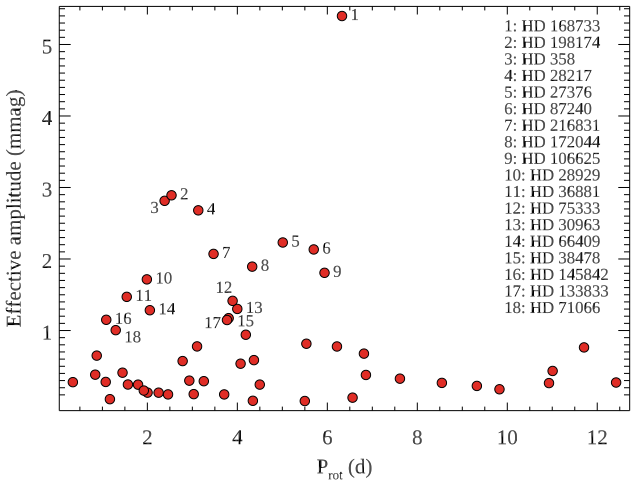

Figure 6. Effective amplitude of the rotational modulation as a function of rotational period. Stars with the largest amplitude of photometric variability are identified in the legend.

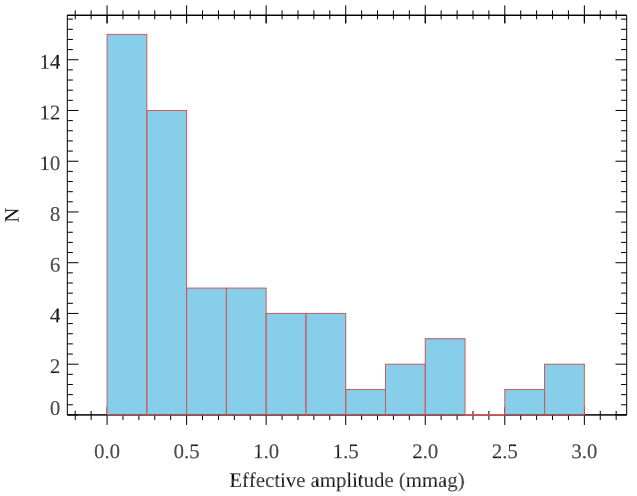

Figure 7. Distribution of the effective variability amplitude for bona fide HgMn stars showing photometric rotational modulation.

The distribution of effective rotational modulation amplitude (Fig. 7) is exponential, with half of the sample stars having an amplitude below 0.54 mmag. This variability is challenging to detect from the ground, which explains why HgMn stars were considered photometrically constant before the advent of space photometry missions (e.g. Adelman 1994b, 1998; Adelman & Meadows 2002). From the comparison of the effective amplitude with the amplitudes of individual harmonics of rotational frequency we can conclude that the shapes of photometric phase curves of HgMn stars are mostly sinusoidal. Only 22 stars (41 per cent of the sample exhibiting rotationally modulated light curves) show deviation from a sinusoidal variability at the level of 30 per cent or more as judged by the difference between the effective amplitude and that of the first harmonic. For 6 stars (11 per cent), the second harmonic dominates over the first one, indicating a double-wave photometric variation. These morphological characteristics of HgMn light curves can be compared to those of magnetic CP (mCP) stars as summarized by

[2] http://gcpd.physics.muni.cz/
[3] http://argonaut.skymaps.info/
[4] https://github.com/Johaney-s/StIFT

Jagelka et al. (2019). These authors found that 67 per cent of mCP stars exhibit single-wave photometric phase curves and 29 per cent have some form of double-wave curves. The latter is somewhat higher than the fraction of double-wave stars derived here, suggesting that HgMn stars have simpler spot distributions than mCP stars. The observed simple photometric phase behaviour of HgMn stars is incompatible with the hypothesis that their surfaces are covered by a complex network of small magnetic spots discussed in the context of magnetic studies of these stars (Hubrig et al. 2012; Kochukhov et al. 2013).

Although our investigation has focused on the analysis of rotational modulation, *TESS* observations allowed us to assess other types of stellar variability. We found 8 HgMn stars (7 objects discussed in Section 4.2 and HD 34923) with multiperiodic pulsations which have amplitude higher or comparable to that of rotational modulation. The 3 stars with 2–5 mmag g-mode oscillations (HD 29589, HD 93549, and HD 171301) are particularly interesting for follow up studies and detailed asteroseismic analyses. All three objects have been studied with high-resolution spectra (Hubrig et al. 2011; Adelman, Gulliver & Gucella 2017; González et al. 2021) and their HgMn classification is indisputable. Two other well-studied HgMn stars, HD 172728 (Adelman, Gulliver & Rayle 2001) and HD 173524 (Adelman, Ryabchikova & Davydova 1998), have the longest *TESS* data sets (12 and 10 *TESS* sectors, respectively). Both stars exhibit g-mode pulsations with amplitudes below 1 mmag. Similar variability is observed in HD 34923. A few other HgMn stars in our survey appear to show weak periodic signal consistent with g-mode pulsation (e.g. HD 11921, HD 27376, HD 110073) in addition to stronger rotational modulation. It is not always clear which of these signals can be attributed to pulsations in HgMn stars and which are caused by blending by nearby faint objects. In any case, we find that high-amplitude g-mode pulsations are rare among HgMn stars, with about 10 per cent of the targets showing this type of variability. The single candidate p-mode pulsator found in this study, HD 145389 (φ Her), is the primary component in a binary system with a late-A star (Zavala et al. 2007). It is likely that the high-frequency pulsational signal is coming from the secondary, which is a δ Sct star. Thus, we find no definite cases of high-frequency oscillation in an HgMn star.

Binarity is another phenomenon responsible for photometric variability of HgMn stars. This includes well-understood eclipse and transit variation in binary systems seen edge-on. In this study, we reported discovery of a possible eclipsing binary with an HgMn component (HD 99803) and another HgMn star (HD 36881) orbited by an eclipsing binary in a hierarchical triple system. Furthermore, the precision of space photometric data enabled detection of new types of variability related to binarity other than eclipses. Here, we identified two HgMn stars, HD 5408 and HD 89822, with heartbeat photometric variability caused by the tidal distortion and tidally induced oscillations excited in the components of an eccentric close binary (e.g. Thompson et al. 2012). Only one case of heartbeat variability in an HgMn star, corresponding to the eclipsing system V680 Mon, was previously known (Paunzen et al. 2021a).

HgMn stars identified in this work as rotational variables are good candidates to search for magnetic fields. It has already been shown that strong magnetic fields like those found in Bp stars are not present in HgMn stars. However, ultra-weak fields could be present. Detecting ultra-weak fields requires very deep spectropolarimetric observations, with an error bar on the longitudinal field measurement of the order of 0.1 G. Such a sensitivity can only be reached with current instrumentation for stars satisfying specific criteria: very bright stars, relatively cool stars (as the spectral type impacts the number and depth of lines that can be used for magnetic measurements), low $v_e \sin i$ (to increase the amplitude of the Zeeman signature in the spectral line), long rotational period (to accumulate more easily measurements in a given rotation phase bin), and no additional variability (such as pulsations or binarity that would blur the magnetic signal). These criteria have already been successfully used to detect ultra-weak fields in Am stars (Blazère et al. 2016). Moreover, it is expected that magnetic field strength decreases at the surface of stars as they evolve, due to magnetic flux conservation (Neiner et al. 2018). Therefore, magnetic field detections require a lower precision for main-sequence stars than for very evolved stars. As a consequence we identify HD 358 (α And), HD 33904 (μ Lep), and HD 106625 (γ Crv) as the best candidates to search for ultra-weak fields in HgMn stars. These targets will be the goal of a future spectropolarimetric study.

ACKNOWLEDGEMENTS

O. Kochukhov acknowledges support by the Swedish Research Council, the Royal Swedish Academy of Sciences, and the Swedish National Space Agency. V. Khalack and O. Kobzar acknowledge support from the Natural Sciences and Engineering Research Council of Canada (NSERC) and from the Faculté des Études Supérieures et de la Recherch de l'Université de Moncton. E. Paunzen acknowledges support by the Erasmus+programme of the European Union under grant number 2020-1-CZ01-KA203-078200. A. David-Uraz acknowledges support by the National Aeronautics and Space Administration (NASA) under award number 80GSFC21M0002. This research has made extensive use of the SIMBAD database, operated at CDS, Strasbourg, France. This work has made use of data from the European Space Agency (ESA) mission *Gaia* (https://www.cosmos.esa.int/gaia), processed by the *Gaia* Data Processing and Analysis Consortium (DPAC, https://www.cosmos.esa.int/web/gaia/dpac/consortium). Funding for the DPAC has been provided by national institutions, in particular the institutions participating in the *Gaia* Multilateral Agreement.

DATA AVAILABILITY

The *TESS* light-curve data underlying this article can be obtained from the Mikulski Archive for Space Telescopes (MAST).

REFERENCES

Abt H. A., Levato H., Grosso M., 2002, ApJ, 573, 359
Adelman S. J., 1994a, MNRAS, 266, 97
Adelman S. J., 1994b, MNRAS, 266, 97
Adelman S. J., 1998, A&AS, 132, 93
Adelman S. J., Brunhouse E. F., 1998, PASP, 110, 1304
Adelman S. J., Gulliver A. F., Gucella L. J., 2017, Astron. Nachr., 338, 584
Adelman S. J., Gulliver A. F., Kochukhov O. P., Ryabchikova T. A., 2002, ApJ, 575, 449
Adelman S. J., Gulliver A. F., Rayle K. E., 2001, A&A, 367, 597
Adelman S. J., Meadows S. A., 2002, A&A, 390, 1023
Adelman S. J., Ryabchikova T. A., Davydova E. S., 1998, MNRAS, 297, 1
Aerts C., Christensen-Dalsgaard J., Kurtz D. W., 2010, Astronomy and Astrophysics Library, Asteroseismology. Springer-Verlag, Berlin
Albayrak B., Ak T., Elmasli A., 2003, Astron. Nachr., 324, 523
Alecian G., 2015, MNRAS, 454, 3143
Alecian G., Gebran M., Auvergne M., Richard O., Samadi R., Weiss W. W., Baglin A., 2009, A&A, 506, 69
Alecian G., Stift M. J., Dorfi E. A., 2011, MNRAS, 418, 986
Alonso M. S., López-García Z., Malaroda S., Leone F., 2003, A&A, 402, 331
Aurière M. et al., 2010, A&A, 523, A40

Babel J., Michaud G., 1991, ApJ, 366, 560
Bagnulo S., Fossati L., Landstreet J. D., Izzo C., 2015, A&A, 583, A115
Bagnulo S., Landstreet J. D., Fossati L., Kochukhov O., 2012, A&A, 538, A129
Bailer-Jones C. A. L., Rybizki J., Fouesneau M., Demleitner M., Andrae R., 2021, AJ, 161, 147
Balona L. A. et al., 2011, MNRAS, 413, 2403
Balona L. A. et al., 2019, MNRAS, 485, 3457
Balona L. A., 2019, MNRAS, 490, 2112
Balona L. A., Baran A. S., Daszyńska-Daszkiewicz J., De Cat P., 2015, MNRAS, 451, 1445
Balona L. A., Ozuyar D., 2020, MNRAS, 493, 5871
Blazère A. et al., 2016, A&A, 586, A97
Breger M. et al., 1993, A&A, 271, 482
Bressan A., Marigo P., Girardi L., Salasnich B., Dal Cero C., Rubele S., Nanni A., 2012, MNRAS, 427, 127
Briquet M., Hubrig S., De Cat P., Aerts C., North P., Schöller M., 2007, A&A, 466, 269
Briquet M., Korhonen H., González J. F., Hubrig S., Hackman T., 2010, A&A, 511, A71
Burssens S. et al., 2020, A&A, 639, A81
Buysschaert B., Neiner C., Briquet M., Aerts C., 2017, A&A, 605, A104
Castelli F., Hubrig S., 2004, A&A, 425, 263
Catanzaro G., Frasca A., Molenda-Żakowicz J., Marilli E., 2010, A&A, 517, A3
Catanzaro G., Giarrusso M., Leone F., Munari M., Scalia C., Sparacello E., Scuderi S., 2016, MNRAS, 460, 1999
Catanzaro G., Giarrusso M., Munari M., Leone F., 2020, MNRAS, 499, 3720
Catanzaro G., Leto P., 2004, A&A, 416, 661
Cayrel de Strobel G., 1996, A&AR, 7, 243
Chojnowski S. D., Hubrig S., Hasselquist S., Beaton R. L., Majewski S. R., García-Hernández D. A., DeColibus D., 2020, MNRAS, 496, 832
Cole W. A., Fekel F. C., Hartkopf W. I., McAlister H. A., Tomkin J., 1992, AJ, 103, 1357
Collado A., López-García Z., 2009, RMxAA, 45, 95
Corbally C. J., 1984, ApJS, 55, 657
Cowley C. R., Hubrig S., Palmeri P., Quinet P., Biémont É., Wahlgren G. M., Schütz O., González J. F., 2010, MNRAS, 405, 1271
Cucchiaro A., Macau-Hercot D., Jaschek M., Jaschek C., 1977, A&AS, 30, 71
Cunha M. S. et al., 2019, MNRAS, 487, 3523
David-Uraz A. et al., 2021, MNRAS, 504, 4841
Dolk L., Wahlgren G. M., Hubrig S., 2003, A&A, 402, 299
Dworetsky M. M., 1982, MNRAS, 199, 303
Flower P. J., 1996, ApJ, 469, 355
Folsom C. P., Kochukhov O., Wade G. A., Silvester J., Bagnulo S., 2010, MNRAS, 407, 2383
Folsom C. P., Wade G. A., Johnson N. M., 2013, MNRAS, 433, 3336
Gaia Collaboration, 2021, A&A, 649, A1
Georgy C., Ekström S., Granada A., Meynet G., Mowlavi N., Eggenberger P., Maeder A., 2013, A&A, 553, A24
Gerbaldi M., Floquet M., Hauck B., 1985, A&A, 146, 341
Ghazaryan S., Alecian G., 2016, MNRAS, 460, 1912
Ghazaryan S., Alecian G., Hakobyan A. A., 2018, MNRAS, 480, 2953
Glagolevskij Y. V., Panov K., Chunakova N. M., 1985, Pisma Astron. Zh., 11, 749
González J. F., Nuñez N. E., Saffe C., Alejo A. D., Veramendi M. E., Collado A., 2021, MNRAS, 502, 3670
Green G. M., Schlafly E., Zucker C., Speagle J. S., Finkbeiner D., 2019, ApJ, 887, 93
Hoffleit D., Warren W. H., Jr, 1991, VizieR Online Data Catalog: Bright Star Catalogue, 5th Revised Ed., Yale University Observatory
Hubrig S. et al., 2010, MNRAS, 408, L61
Hubrig S. et al., 2011, Astron. Nachr., 332, 998
Hubrig S. et al., 2012, A&A, 547, A90
Hubrig S. et al., 2014, MNRAS, 442, 3604
Hubrig S., González J. F., Savanov I., Schöller M., Ageorges N., Cowley C. R., Wolff B., 2006, MNRAS, 371, 1953
Hubrig S., Järvinen S. P., Korhonen H., Ilyin I., Schöller M., Niemczura E., Chojnowski S. D., 2020, MNRAS, 495, L97
Hubrig S., Le Mignant D., North P., Krautter J., 2001, A&A, 372, 152
Hummel C. A., Schöller M., Duvert G., Hubrig S., 2017, A&A, 600, L5
Hümmerich S., Niemczura E., Walczak P., Paunzen E., Bernhard K., Murphy S. J., Drobek D., 2018, MNRAS, 474, 2467
Hutchings J. B., Nemec J. M., Cassidy J., 1979, PASP, 91, 313
Ilyin I. V., 2000, PhD thesis. Univ. Oulu, Finland
Jagelka M., Mikulášek Z., Hümmerich S., Paunzen E., 2019, A&A, 622, A199
Jenkins J. M. et al., 2016, in Chiozzi G., Guzman J. C., eds, SPIE Conf. Ser. Vol. 9913, Software and Cyberinfrastructure for Astronomy IV. SPIE, Bellingham, p. 99133E
Kammerer J., Ireland M. J., Martinache F., Girard J. H., 2019, MNRAS, 486, 639
Kochukhov O. et al., 2011, A&A, 534, L13
Kochukhov O. et al., 2013, A&A, 554, A61
Kochukhov O., Adelman S. J., Gulliver A. F., Piskunov N., 2007, Nat. Phys., 3, 526
Kochukhov O., Bagnulo S., 2006, A&A, 450, 763
Kochukhov O., Drake N. A., Piskunov N., de la Reza R., 2004, A&A, 424, 935
Kochukhov O., Johnston C., Labadie-Bartz J., Shetye S., Ryabchikova T. A., Tkachenko A., Shultz M. E., 2021, MNRAS, 500, 2577
Kochukhov O., Lüftinger T., Neiner C., Alecian E., MiMeS Collaboration, 2014, A&A, 565, A83
Kochukhov O., Piskunov N., Sachkov M., Kudryavtsev D., 2005, A&A, 439, 1093
Kochukhov O., Shultz M., Neiner C., 2019, A&A, 621, A47
Korhonen H. et al., 2013, A&A, 553, A27
Krtička J. et al., 2020, A&A, 639, A8
Kuschnig R., Weiss W. W., Gruber R., Bely P. Y., Jenkner H., 1997, A&A, 328, 544
Le Bouquin J. B., Beust H., Duvert G., Berger J. P., Ménard F., Zins G., 2013, A&A, 551, A121
LeBlanc F., Monin D., Hui-Bon-Hoa A., Hauschildt P. H., 2009, A&A, 495, 937
Makaganiuk V. et al., 2011a, A&A, 525, A97
Makaganiuk V. et al., 2011b, A&A, 529, A160
Makaganiuk V. et al., 2012, A&A, 539, A142
Markwardt C. B., 2009, in Bohlender D. A., Durand D., Dowler P., eds, ASP Conf. Ser. Vol. 411, Astronomical Data Analysis Software and Systems XVIII. Astron. Soc. Pac., San Francisco, p. 251
Martin A. J. et al., 2018, MNRAS, 475, 1521
Mathys G., 1994, A&AS, 108, 547
Mathys G., Hubrig S., 1997, A&AS, 124, 475
Michaud G., 1982, ApJ, 258, 349
Michaud G., Alecian G., Richer J., 2015, Atomic Diffusion in Stars. Springer International Publishing, Switzerland
Michaud G., Megessier C., Charland Y., 1981, A&A, 103, 244
Mikulášek Z., Janík J., Zverko J., Žižňovský J., Zejda M., Netolický M., Vaňko M., 2007, Astron. Nachr., 328, 10
Monier R., Gebran M., Royer F., 2015, A&A, 577, A96
Monier R., Griffin E., Gebran M., Kılıçoğlu T., Merle T., Royer F., 2019, AJ, 158, 157
Morel T. et al., 2014, A&A, 561, A35
Mowlavi N., Saesen S., Semaan T., Eggenberger P., Barblan F., Eyer L., Ekström S., Georgy C., 2016, A&A, 595, L1
Napiwotzki R., Schoenberner D., Wenske V., 1993, A&A, 268, 653
Neiner C., Martin A., Wade G., Oksala M., 2018, in Di Matteo P., Billebaud F., Herpin F., Lagarde N., Marquette J. B., Robin A., Venot O., eds, SF2A-2018: Proceedings of the Annual meeting of the French Society of Astronomy and Astrophysics. French Society of Astronomy and Astrophysics, Paris, p. 319
Netopil M., Paunzen E., Hümmerich S., Bernhard K., 2017, MNRAS, 468, 2745
Netopil M., Paunzen E., Maitzen H. M., North P., Hubrig S., 2008, A&A, 491, 545

Nuñez N. E., González J. F., Hubrig S., 2011, in Kudryavtsev D. O., Romanyuk I. I., Zyazeva A. V., eds, Magnetic Stars. Special Astrophysical Observatory, Nizhny Arkhyz, p. 109
Paunzen E., 2015, A&A, 580, A23
Paunzen E., Huemmerich S., Fedurco M., Bernhard K., Komzik R., Vanko M., 2021a, MNRAS, 504, 3749
Paunzen E., Hümmerich S., Bernhard K., 2021b, A&A, 645, A34
Paunzen E., Schnell A., Maitzen H. M., 2006, A&A, 458, 293
Paunzen E., Wraight K. T., Fossati L., Netopil M., White G. J., Bewsher D., 2013, MNRAS, 429, 119
Pecaut M. J., Mamajek E. E., 2013, ApJS, 208, 9
Pedersen M. G. et al., 2019, ApJ, 872, L9
Petit P. et al., 2010, A&A, 523, A41
Petit P. et al., 2011, A&A, 532, L13
Pope B. J. S. et al., 2019, ApJS, 245, 8
Pourbaix D. et al., 2004, A&A, 424, 727
Pourbaix D., Boffin H. M. J., Chini R., Dembsky T., 2013, A&A, 556, A45
Preston G. W., 1974, ARA&A, 12, 257
Prvák M., Krtička J., Korhonen H., 2020, MNRAS, 492, 1834
Renson P., Manfroid J., 2009, A&A, 498, 961
Ricker G. R. et al., 2015, J. Astron. Telesc. Instrum. Syst., 1, 014003
Riello M. et al., 2021, A&A, 649, A3
Roby S. W., Lambert D. L., 1990, ApJS, 73, 67
Ryabchikova T. A., Piskunov N. E., Stempels H. C., Kupka F., Weiss W. W., 1999, Phys. Scr. T, 83, 162
Ryabchikova T. A., Zakharova L. A., Adelman S. J., 1996, MNRAS, 283, 1115
Schneider H., 1981, A&AS, 44, 137
Schöller M., Correia S., Hubrig S., Ageorges N., 2010, A&A, 522, A85
Shorlin S. L. S., Wade G. A., Donati J.-F., Landstreet J. D., Petit P., Sigut T. A. A., Strasser S., 2002, A&A, 392, 637
Shultz M. E., Rivinius T., Wade G. A., Kochukhov O., Alecian E., David-Uraz A., Sikora J., MiMeS Collaboration, 2021, MNRAS , 504, 4850
Sikora J., Wade G. A., Rowe J., 2020, MNRAS, 498, 2456
Stassun K. G. et al., 2019, AJ, 158, 138
Strassmeier K. G. et al., 2020, A&A, 644, A104
Strassmeier K. G., Granzer T., Mallonn M., Weber M., Weingrill J., 2017, A&A, 597, A55
Thompson S. E. et al., 2012, ApJ, 753, 86
Tsymbal V. V., Kotchukhov O. P., Khokhlova V. L., Lambert D. L., 1998, Astron. Lett., 24, 90
van Belle G. T., 2012, A&AR, 20, 51
van Leeuwen F., 2007, A&A, 474, 653
Wade G. A. et al., 2006, A&A, 451, 293
White T. R. et al., 2017, MNRAS, 471, 2882
Woolf V. M., Lambert D. L., 1999, ApJ, 521, 414
Yüce K., Adelman S. J., 2014, PASP, 126, 345
Yushchenko A. V., Gopka V. F., Khokhlova V. L., Musaev F. A., Bikmaev I. F., 1999, Astron. Lett., 25, 453
Zavala R. T. et al., 2007, ApJ, 655, 1046
Zechmeister M., Kürster M., 2009, A&A, 496, 577
Zorec J., Royer F., 2012, A&A, 537, A120
Zverko J., Ziznovsky J., Khokhlova V. L., 1997, Contrib. Astron. Obs. Skalnate Pleso, 27, 41

APPENDIX A: TIME SERIES ANALYSIS RESULTS

Table A1. Results of time series analysis of *TESS* light curves of HgMn stars. The columns give the HD number for every target, other commonly used name, the TIC identification number, *V* magnitude, analysed sectors, periods, and amplitudes of variability. Harmonic signals are indicated by '/' followed by the harmonic number. Uncertainties in the last significant digits are indicated in parentheses for periods and amplitudes. The last column highlights periods attributed to rotational modulation or binarity.

HD	Other id.	TIC	*V* (mag)	Sectors	*P* (d)	*A* (mmag)	Comment
358	α And	427733653	2.070	17	2.38337(17)	2.8136(41)	ROT
1009		83803744	8.400	17,18	2.24978(96)	0.0697(42)	ROT
					/2	0.1106(42)	
					0.0808487(67)	0.0426(41)	
					0.0461809(33)	0.0283(41)	
					0.0449932(36)	0.0245(41)	
1279	HR 62	440076466	5.858	17	7.614(11)	0.3021(50)	ROT
					/2	0.1118(32)	
					/3	0.0542(31)	
4382	23 Cas	275361674	5.422	18,19	11.0079(76)	0.4343(28)	ROT?
					6.1938(39)	0.2544(23)	
5408	HR 266	51961599	5.562	17,18	6.357(12)	0.0724(20)	
					4.24074(16)	0.0611(21)	heartbeat
					/2	0.1837(19)	
					/3	0.2748(19)	
					/4	0.2456(19)	
					/5	0.2115(19)	
					/6	0.0949(19)	
					/7	0.1146(19)	
					/8	0.0819(19)	
					/9	0.0526(19)	
					/10	0.0307(19)	
					/11	0.0196(19)	
11291	2 Per	285425945	5.702	18	6.384(17)	0.1865(34)	
					3.9369(46)	0.2769(33)	
					2.78350(99)	0.5725(32)	ROT?
11753	φ Phe	229099027	5.120	3	9.3238(82)	0.0833(18)	ROT
					/2	0.2031(18)	
					/3	0.0446(18)	
					/4	0.0227(18)	

Table A1 – *continued*

HD	Other id.	TIC	V (mag)	Sectors	P (d)	A (mmag)	Comment
14228	φ Eri	354671857	3.560	2,3	0.461391(57)	0.03292(88)	
					0.454053(59)	0.03081(88)	
					0.3437583(35)	0.27766(82)	ROT
16727	11 Per	245758891	5.761	18	11.706(14)	0.7451(92)	ROT
					/2	0.1669(45)	
19400	θ Hyi	280051467	5.510	1,2,13	4.368500(45)	0.5826(13)	ROT
					/2	0.0626(13)	
27376	41 Eri	168847194	3.550	4,5	5.00966(19)	2.1838(17)	ROT
					/2	0.4563(17)	
					0.773022(16)	0.6515(17)	
28217	HR 1402	373026963	5.872	5	3.13164(30)	2.6615(39)	ROT
					/2	0.3186(39)	
					2.3540(11)	0.4335(39)	
28929	HR 1445	268507411	5.894	19	1.98864(15)	1.6861(31)	ROT
					/2	0.3144(31)	
29589	93 Tau	245936817	5.455	5	1.56746(77)	0.2448(37)	ROT?
					0.754386(90)	0.5583(37)	
					0.703415(26)	1.9520(40)	
					0.67346(11)	0.4339(42)	
					0.643669(21)	1.8721(41)	
					0.610245(48)	0.6492(39)	
					0.546276(18)	1.3110(37)	
					0.344503(35)	0.2621(37)	
					0.329194(48)	0.1759(37)	
					0.272684(15)	0.3886(37)	
30963		9355205	7.265	5	3.99912(90)	1.2976(36)	ROT
					/2	0.1054(36)	
31373	HR 1576	436723855	5.791	5	2.6438(35)	0.0876(22)	
					1.44772(19)	0.3817(21)	ROT
					/2	0.1503(21)	
32964	66 Eri	248396674	5.097	5	5.5347(10)	0.6415(21)	ROT?
					/2	0.4928(20)	
					/3	0.0977(20)	
					/4	0.0269(20)	
33904	μ Lep	169534653	3.290	5	2.9327(11)	0.2903(21)	ROT
					/2	0.0712(21)	
					0.46771(19)	0.0501(21)	
34364	AR Aur	2236015	6.147	19	4.134	$\approx$600	Eclipses
34923		2776520	9.734	19	0.7485(17)	0.072(11)	Single transit
					0.50543(53)	0.109(11)	
					0.252364(56)	0.255(10)	
36881	HR 1883	436103335	5.604	6	1.54148(20)	1.4404(53)	ROT
					/2	0.2978(52)	
					1.16825(53)	0.3384(53)	
					7.86		Eclipses
37437		116154521	8.129	19	6.858(10)	0.3289(58)	ROT
					/2	0.1663(58)	
					/3	0.0863(57)	
37519	HR 1938	116333643	6.040	19	0.840782(85)	0.3295(29)	ROT
					/2	0.1885(29)	
					/3	0.0410(29)	
					/4	0.0218(29)	
37886		11411002	8.979	6	4.0719(69)	0.5361(87)	ROT?
					2.5140(46)	0.3021(86)	
38478	129 Tau	247638066	6.010	6	3.8065(12)	1.1621(35)	ROT
					/2	0.1579(35)	
49606	33 Gem	155095401	5.855	6	8.546(13)	0.1808(32)	ROT
					/2	0.1972(31)	
53244	γ CMa	148109427	4.110	7	7.8042(90)	0.3702(17)	
					6.2140(27)	0.7720(16)	ROT
					/2	0.0846(15)	
65950		372913233	6.860	1,2,7-11	$>$0.5	$<$0.0463	
66409		410451677	8.373	1,7-11	2.055116(15)	1.2783(26)	ROT
					/2	0.1174(26)	

Table A1 – *continued*

HD	Other id.	TIC	V (mag)	Sectors	P (d)	A (mmag)	Comment
69028		139271386	7.990	20	6.8137(46)	0.4711(60)	ROT
					/2	0.4738(58)	
					/3	0.1086(57)	
71066	κ^2 Vol	307291308	5.630	5,6,10-13	1.2963766(63)	1.0050(19)	ROT
75333	14 Hya	62480591	5.291	8	3.89443(75)	1.4147(35)	ROT
76728	c Car	356299294	3.840	10	4.1880(11)	0.9409(26)	ROT
77350	ν Cnc	126349649	5.456	21	>0.5	<0.2462	
80078		357981882	8.203	9-11	10.9274(58)	0.1642(38)	ROT
					/2	0.2076(32)	
87240		462162948	9.650	9,10	5.6980(15)	2.1335(95)	ROT
89822	HR 4072	287287930	4.950	14,21	11.58105(53)	0.2638(39)	Hearbeat
					/2	0.2939(25)	
					/3	0.2091(24)	
					/4	0.0980(24)	
					/5	0.0561(23)	
					/6	0.0385(23)	
93549	HR 4220	391421890	5.230	10,11	5.6537(35)	0.1932(22)	
					3.72367(54)	0.5346(21)	
					2.89581(46)	0.3709(21)	
					1.93136(29)	0.2526(20)	
					1.44737(24)	0.1708(20)	
					0.874401(23)	0.6476(20)	ROT
					/2	0.0429(20)	
99803	HR 4423	163024899	5.140	10		≈46	Single eclipse
101189	HR 4487	319809753	5.150	10,11	2.00407(53)	0.1312(18)	ROT
101391	HR 4493	137752707	6.353	21	1.07428(20)	0.2787(25)	ROT
					/2	0.0332(25)	
					/3	0.0097(25)	
106625	γ Crv	348987372	2.580	10	5.9377(15)	1.8000(39)	ROT
					/2	0.1572(38)	
110073	HR 4817	144395071	4.630	10	5.903(11)	0.1122(17)	
					3.0301(27)	0.1066(17)	ROT?
					/2	0.0280(16)	
					2.3479(31)	0.0599(16)	
					1.3414(12)	0.0534(16)	
133833		121161014	8.225	12	3.7700(16)	1.1373(72)	ROT
					/2	0.1477(70)	
141556	χ Lup	442652828	3.970	12	1.79286(54)	0.2429(19)	ROT
143807	ι CrB	356010327	4.978	24,25	>0.5	<0.0313	
144206	υ Her	417582433	4.723	23-25	>0.5	<0.0221	
145389	φ Her	219480018	4.237	25	4.446(16)	0.0424(13)	
					3.7076(29)	0.0990(14)	ROT
					/2	0.0049(13)	
					/3	0.0381(13)	
					0.0546655(55)	0.0144(13)	
					0.0527289(33)	0.0222(13)	
					0.05097180(75)	0.0924(13)	
					0.0493830(42)	0.0156(13)	
					0.0465250(51)	0.0112(13)	
					0.0448131(49)	0.0109(13)	
145842	θ Nor	51612589	5.130	12	1.08588(13)	1.1444(60)	ROT
					/2	0.1119(60)	
156127		198388195	8.300	14-26	2.45915(14)	0.1065(16)	ROT
					0.694363(50)	0.0237(16)	
					0.688940(20)	0.0395(16)	
					/2	0.0126(16)	
					/3	0.0113(16)	
					0.683537(44)	0.0262(16)	
					0.678268(64)	0.0177(16)	
156678		198409372	8.632	14-25	4.3448(34)	0.0172(19)	ROT?
					0.388511(21)	0.0223(18)	
169027	38 Dra	236770286	6.784	14-26	1.21850(19)	0.01119(97)	
					1.167052(50)	0.03959(97)	ROT?
168733	HR 6870	323999777	5.330	13	6.32604(88)	5.3980(55)	ROT
171301	HR 6968	27697099	5.478	26	3.10449(96)	0.7775(35)	ROT?

Table A1 *– continued*

HD	Other id.	TIC	V (mag)	Sectors	P (d)	A (mmag)	Comment
					0.947931(35)	1.9107(34)	
					0.795271(11)	4.1444(34)	
					0.633192(60)	0.4981(34)	
172044	HR 6997	27901267	5.409	26	4.33023(84)	1.7691(42)	ROT
					/2	0.6662(40)	
					/3	0.0910(39)	
					/4	0.0579(39)	
					3.6797(74)	0.2179(40)	
					1.00444(69)	0.1264(39)	
172728	HR 7018	383676357	5.746	14-26	4.498374(95)	0.24364(76)	ROT
					2.76518(16)	0.05519(75)	
					2.606514(75)	0.10438(76)	
					2.533836(88)	0.09821(79)	
					2.512467(99)	0.08684(79)	
					1.258558(37)	0.04831(75)	
173524	46 Dra	392569763	5.030	15,16,18-23,25,26	9.82663(47)	0.15617(78)	ROT
					/2	0.07340(72)	
					/3	0.04465(71)	
					1.447225(18)	0.14437(72)	
					1.0131045(67)	0.18481(71)	
					0.722427(16)	0.03865(71)	
174933	112 Her	347160134	5.430	26	12.419(17)	0.1153(66)	ROT
					/2	0.2385(36)	
					/3	0.0652(27)	
198174	HR 7961	270070443	5.860	1	2.53650(21)	2.8910(46)	ROT
202033		76960308	8.470	15	>0.5	<0.0685	
212093		422012928	8.266	16,17	6.561(24)	0.0422(47)	ROT?
					/2	0.0443(45)	
216831	HR 8723	129533458	5.743	16	3.4709(13)	2.0713(96)	ROT
219485	HR 8844	417703090	5.899	17,19,24,25	5.4993(41)	0.0141(11)	ROT?
					3.9488(24)	0.0122(11)	
					2.5276(11)	0.0102(10)	
221507	β Scl	224244458	4.380	2	1.92060(45)	0.15928(99)	ROT
					/2	0.01832(99)	
					0.65573(12)	0.05919(99)	ROT companion
					/2	0.01677(99)	
225289	HR 9110	359033491	5.783	17,18	3.25423(85)	0.2733(27)	ROT
					/2	0.0931(27)	
					/3	0.0384(27)	

APPENDIX B: STELLAR PARAMETERS

Table B1. Essential data for HgMn stars with rotational periods measured in our study. The columns denote: (1) HD number, (2) V magnitude, (3) distance, (4) logarithmic effective temperature, (5) bolometric correction, (6) logarithmic luminosity, (7) radius, (8) observed period, (9) calibrated equatorial velocity, (10) critical velocity, (11) ratio of the calibrated equatorial velocity, and critical velocity.

(1) HD	(2) V (mag)	(3) D (pc)	(4) $\log T_{\rm eff}$ (K)	(5) BC (mag)	(6) $\log L/L_\odot$	(7) R ($R_\odot$)	(8) $P_{\rm rot}$ (d)	(9) $v_{\rm eq}$ (km s^{-1})	(10) $v_{\rm crit}$ (km s^{-1})	(11) $v_{\rm eq}/v_{\rm crit}$
358	2.070	29.7 ± 0.3	4.129 ± 0.004	−0.975	2.429 ± 0.007	3.031	2.383	64	383	0.17
1009	8.400	554.0 ± 6.2	4.081 ± 0.002	−0.695	2.670 ± 0.007	4.980	2.250	112	324	0.35
1279	5.858	347.4 ± 6.7	4.114 ± 0.004	−0.887	3.044 ± 0.009	6.572	7.614	44	348	0.13
4382	5.422	239.9 ± 2.9	4.110 ± 0.006	−0.862	2.901 ± 0.007	5.678	11.008	26	303	0.09
11291	5.702	145.9 ± 2.3	4.067 ± 0.005	−0.614	2.227 ± 0.008	3.189	2.784	58	362	0.16
11753	5.120	98.2 ± 1.8	4.027 ± 0.013	−0.385	1.990 ± 0.009	2.922	9.324	16	330	0.05
14228	3.560	46.1 ± 0.5	4.102 ± 0.004	−0.814	2.129 ± 0.007	2.422	0.344	356	409	0.87
16727	5.761	128.2 ± 1.2	4.144 ± 0.005	−1.057	2.255 ± 0.007	2.312	11.706	10	420	0.02
19400	5.510	153.8 ± 1.4	4.133 ± 0.003	−0.995	2.468 ± 0.007	3.108	4.369	36	359	0.10
27376	3.550	54.5 ± 0.7	4.100 ± 0.001	−0.804	2.274 ± 0.008	2.898	5.010	29	407	0.07
28217	5.872	321.1 ± 54.2	4.127 ± 0.002	−0.960	3.183 ± 0.066	7.269	3.132	117	296	0.40
28929	5.894	138.3 ± 0.9	4.103 ± 0.001	−0.820	2.226 ± 0.006	2.708	1.989	69	366	0.19
29589	5.455	120.6 ± 1.8	4.147 ± 0.005	−1.076	2.311 ± 0.008	2.435	1.567	79	394	0.20
30963	7.265	310.9 ± 3.0	4.069 ± 0.001	−0.623	2.289 ± 0.007	3.400	3.999	43	338	0.13
31373	5.791	140.2 ± 2.5	4.130 ± 0.003	−0.980	2.304 ± 0.009	2.615	1.448	91	396	0.23
32964	5.097	93.1 ± 1.0	4.046 ± 0.005	−0.492	1.999 ± 0.007	2.707	5.535	25	395	0.06
33904	3.290	52.0 ± 0.9	4.097 ± 0.005	−0.788	2.333 ± 0.009	3.138	2.933	54	380	0.14
36881	5.604	500.8 ± 25.6	4.039 ± 0.015	−0.451	3.526 ± 0.021	16.171	1.541	531	200	2.65
37437	8.129	532.0 ± 16.1	4.133 ± 0.006	−0.995	2.571 ± 0.013	3.500	6.858	26	380	0.07
37519	6.040	239.2 ± 2.8	4.062 ± 0.006	−0.584	2.656 ± 0.007	5.343	0.841	321	333	0.97
37886	8.979	365.0 ± 4.9	4.092 ± 0.002	−0.755	1.814 ± 0.008	1.800	4.072	22	459	0.05
38478	6.010	270.5 ± 5.8	4.116 ± 0.003	−0.895	2.758 ± 0.010	4.684	3.807	62	367	0.17
49606	5.855	204.5 ± 3.8	4.136 ± 0.003	−1.015	2.591 ± 0.009	3.530	8.546	21	374	0.06
53244	4.110	130.1 ± 3.2	4.122 ± 0.005	−0.933	2.873 ± 0.011	5.205	6.214	42	329	0.13
66409	8.373	424.8 ± 8.7	4.103 ± 0.003	−0.824	2.291 ± 0.010	2.907	2.055	72	399	0.18
69028	7.990	436.0 ± 9.8	4.039 ± 0.002	−0.453	2.274 ± 0.010	3.829	6.814	28	333	0.09
71066	5.630	126.2 ± 1.0	4.077 ± 0.004	−0.670	2.118 ± 0.006	2.696	1.296	105	357	0.29
75333	5.291	131.0 ± 1.8	4.081 ± 0.004	−0.693	2.339 ± 0.008	3.402	3.894	44	331	0.13
76728	3.840	89.3 ± 2.3	4.120 ± 0.003	−0.918	2.649 ± 0.011	4.057	4.188	49	398	0.12
80078	8.203	479.1 ± 5.0	4.110 ± 0.007	−0.864	2.350 ± 0.007	3.022	10.927	14	372	0.04
87240	9.650	1341.7 ± 134.0	4.108 ± 0.008	−0.850	2.694 ± 0.039	4.520	5.698	40	327	0.12
93549	5.230	149.8 ± 2.2	4.148 ± 0.006	−1.083	2.657 ± 0.008	3.606	0.874	209	398	0.52
101189	5.150	96.1 ± 1.3	4.045 ± 0.008	−0.488	2.038 ± 0.008	2.848	2.004	72	379	0.19
101391	6.353	153.3 ± 0.9	4.087 ± 0.003	−0.728	2.024 ± 0.006	2.305	1.074	109	378	0.29
106625	2.580	47.1 ± 0.4	4.076 ± 0.004	−0.661	2.479 ± 0.007	4.087	5.938	35	306	0.11
110073	4.630	101.8 ± 2.1	4.107 ± 0.004	−0.842	2.454 ± 0.010	3.446	3.030	58	332	0.17
133833	8.225	332.8 ± 50.3	4.084 ± 0.002	−0.712	1.963 ± 0.059	2.185	3.770	29	403	0.07
141556	3.970	62.6 ± 1.5	4.030 ± 0.009	−0.402	2.069 ± 0.011	3.161	1.793	89	349	0.26
145389	4.237	73.7 ± 2.6	4.065 ± 0.006	−0.599	2.222 ± 0.015	3.203	3.708	44	363	0.12
145842	5.130	111.7 ± 1.3	4.099 ± 0.003	−0.800	2.264 ± 0.007	2.879	1.086	134	410	0.33
156127	8.300	417.9 ± 4.4	4.025 ± 0.010	−0.376	2.070 ± 0.007	3.237	2.459	67	345	0.19
156678	8.632	330.4 ± 2.3	3.977 ± 0.011	−0.145	1.580 ± 0.006	2.290	4.345	27	330	0.08
168733	6.784	197.2 ± 3.9	4.120 ± 0.011	−0.920	2.164 ± 0.010	2.332	1.167	101	396	0.26
169027	5.330	178.7 ± 1.0	4.057 ± 0.006	−0.556	2.495 ± 0.006	4.546	6.326	36	303	0.12
171301	5.478	106.9 ± 0.7	4.086 ± 0.002	−0.724	2.074 ± 0.006	2.461	3.104	40	355	0.11
172044	5.409	162.8 ± 1.8	4.143 ± 0.003	−1.051	2.625 ± 0.007	3.556	4.330	42	410	0.10
172728	5.746	128.2 ± 1.4	4.035 ± 0.010	−0.431	2.011 ± 0.007	2.884	4.498	32	389	0.08
173524	5.030	110.3 ± 1.0	4.061 ± 0.005	−0.580	2.215 ± 0.007	3.240	9.827	17	325	0.05
174933	5.430	127.3 ± 1.2	4.109 ± 0.003	−0.858	2.308 ± 0.007	2.888	12.419	12	391	0.03
198174	5.860	149.9 ± 3.7	4.114 ± 0.004	−0.887	2.330 ± 0.011	2.901	2.537	58	382	0.15
212093	8.266	317.9 ± 11.3	4.090 ± 0.007	−0.745	1.957 ± 0.015	2.106	6.561	16	407	0.04
216831	5.743	217.8 ± 4.6	4.107 ± 0.005	−0.844	2.684 ± 0.010	4.488	3.471	65	334	0.20
219485	5.899	136.3 ± 1.0	3.999 ± 0.012	−0.243	1.909 ± 0.006	3.025	5.499	28	324	0.09
221507	4.380	55.9 ± 0.7	4.093 ± 0.007	−0.764	1.948 ± 0.008	2.054	1.921	54	411	0.13
225289	5.783	209.9 ± 2.1	4.104 ± 0.005	−0.826	2.628 ± 0.007	4.270	3.254	66	350	0.19

This paper has been typeset from a TEX/LATEX file prepared by the author.